

Unified Framework for Open Quantum Dynamics with Memory

Felix Ivander,¹ Lachlan P. Lindoy,² and Joonho Lee^{3,4,*}

¹Quantum Science and Engineering, Harvard University, Cambridge, MA, USA

²National Physical Laboratory, Teddington, TW11 0LW, United Kingdom

³Department of Chemistry and Chemical Biology, Harvard University, Cambridge, MA, USA

⁴Google Quantum AI, Venice, CA, USA

Studies of the dynamics of a quantum system coupled to a bath are typically performed by utilizing the Nakajima-Zwanzig memory kernel (\mathcal{K}) or the influence functions (\mathbf{I}), especially when the dynamics exhibit memory effects (i.e., non-Markovian). Despite their significance, the formal connection between the memory kernel and the influence functions has not been explicitly made. We reveal their relation through the observation of a diagrammatic structure underlying the system propagator, \mathbf{I} , and \mathcal{K} . Based on this, we propose a non-perturbative, diagrammatic approach to construct \mathcal{K} from \mathbf{I} for (driven) systems interacting with harmonic baths without the use of any projection-free dynamics inputs required by standard approaches. With this construction, we also show how approximate path integral methods can be understood in terms of approximate memory kernels. Furthermore, we demonstrate a Hamiltonian learning procedure to extract the bath spectral density from a set of reduced system trajectories obtained experimentally or by numerically exact methods, opening new avenues in quantum sensing and engineering. The insights we provide in this work will significantly advance the understanding of non-Markovian dynamics, and they will be an important stepping stone for theoretical and experimental developments in this area.

Introduction. Most existing quantum systems inevitably interact with the surrounding environment, often making a straightforward application of Schrödinger's equation impractical.¹ The main challenge in modeling these “open” quantum systems is the large Hilbert space dimension because the environment is much larger than the system of interest. Addressing this challenge is important in many disciplines, including solid state and condensed matter physics,^{2–4} chemical physics and quantum biology,^{5–8} quantum optics,^{9–12} and quantum information science.^{13–15} Despite significant research efforts in this area,^{16–18} an efficient and completely general description of open quantum dynamics, especially those with memory (i.e., non-Markovianity), is yet to be found. In this Article, we provide a unified framework for studying non-Markovian open quantum systems, which will help to facilitate a better understanding of open quantum dynamics and the development of numerical methods.

To describe *non-Markovian* open quantum dynamics, various numerically exact methods have been developed. Two of the most commonly used approaches are (1) the Feynman-Vernon influence functional path integral (INFPI)¹⁹ based techniques, including the quasiadiabatic path-integral method of Makri and Makarov and its variants^{20–29}, hierarchical equations of motion (HEOM) methods,^{7,30,31} and time-evolving matrix product operator and related process tensor based approaches,^{18,32–34} and (2) the Nakajima-Zwanzig generalized quantum master equation (GQME) techniques.^{35–38} The INFPI formulation employs the influence functional (\mathcal{I}) that encodes the time-nonlocal influence of the baths on the system. In the GQME formalism, the analogous object to \mathcal{I} is the memory kernel (\mathcal{K}), which describes the entire complexity of the bath influence on the reduced system dynamics. It is natural to intuit that \mathcal{I} and \mathcal{K} are closely connected and are presumably identical in their information con-

tent. Despite this, to the best of our knowledge *analytic* and *explicit* relationships between the two have yet to be shown.

There have been several works that loosely connect these two frameworks. For instance, there is a body of work on numerically computing \mathcal{K} with projection-free inputs using short-time system trajectories based on INFPI or other exact quantum dynamics methods.^{39–42} The obtained \mathcal{K} is then used to propagate system dynamics to longer times. Another line of work worth noting is the real-time path integral Monte Carlo algorithms for evaluating memory kernels exactly.⁴³ These works took advantage of the real-time path integral approaches used to evaluate \mathcal{I} ⁴⁴ to evaluate necessary matrix elements in computing the exact memory kernel. Nonetheless, they did not present any direct analytical relationship between the memory kernel and \mathcal{I} . In this Article, we present a unifying description of these non-Markovian quantum dynamics frameworks. In particular, we establish explicit *analytic correspondence* between \mathcal{I} and \mathcal{K} . We present a visual schematic describing the main idea of our work in Fig. 1 panel (a).

Path Integral Formulation. We consider a system described by the Hamiltonian \hat{H}_S coupled to a bath that is described by a bosonic quadratic Hamiltonian, $\hat{H}_B = \sum_k \omega_k \hat{b}_k^\dagger \hat{b}_k$. For simplicity, we limit our discussion to a linear system-bath coupling, $\hat{H}_I = \hat{S} \otimes \hat{B}$ where \hat{S} is a system operator that is diagonal in the computational basis and $\hat{B} = \sum_k \lambda_k (\hat{b}_k^\dagger + \hat{b}_k)$ is a bath operator that is linear in the bath creation and annihilation operators. The total Hamiltonian is therefore $\hat{H} = \hat{H}_S + \hat{H}_B + \hat{H}_I$, governing the time evolution of the full system, $\rho_{\text{tot}}(t) = e^{-i\hat{H}t} \rho_{\text{tot}}(0) e^{i\hat{H}t}$. We discretize time and employ a Trotterized propagator,

$$e^{-i\hat{H}\Delta t} = e^{-i\hat{H}_S\Delta t/2} e^{-i\hat{H}_{\text{env}}\Delta t} e^{-i\hat{H}_S\Delta t/2} + O(\Delta t^3), \quad (1)$$

where $\hat{H}_{\text{env}} = \hat{H} - \hat{H}_S$. The initial total density matrix is assumed to be factorized into $\rho_{\text{tot}}(0) = \rho(0) \otimes Z^{-1} \exp[-\beta \hat{H}_B]$ at inverse temperature β where $Z = \text{Tr} \left\{ \exp[-\beta \hat{H}_B] \right\}$. Then, one can show that the dynamics of the reduced system density matrix, $\rho(N\Delta t) = \rho_N = \text{Tr}_B [\rho_{\text{tot}}(N\Delta t)]$, follows

$$\begin{aligned} \langle x_{2N}^+ | \rho_N | x_{2N}^- \rangle &= \sum_{x_0^\pm \cdots x_{2N-1}^\pm} G_{x_0^\pm x_1^\pm} G_{x_1^\pm x_2^\pm} \cdots G_{x_{2N-1}^\pm x_{2N}^\pm} \\ &\times \langle x_0^+ | \rho_0 | x_0^- \rangle \mathcal{I}(x_1^\pm, x_3^\pm, \dots, x_{2N-1}^\pm), \end{aligned} \quad (2)$$

where $G_{x_m^\pm x_{m+1}^\pm} = \langle x_m^+ | e^{-\frac{i\hat{H}_S \Delta t}{2}} | x_{m+1}^+ \rangle \langle x_{m+1}^- | e^{\frac{i\hat{H}_S \Delta t}{2}} | x_m^- \rangle$. From this, we can show that the influence functional, \mathcal{I} , is pairwise separable,

$$\begin{aligned} \mathcal{I}(x_1^\pm, x_3^\pm, \dots, x_{2N-1}^\pm) &= \prod_{n=1}^N I_{0, x_{2n-1}^\pm} \prod_{n=1}^{N-1} I_{1, x_{2n-1}^\pm x_{2n+1}^\pm} \\ &\times \prod_{n=2}^{N-1} I_{2, x_{2n-3}^\pm x_{2n+1}^\pm} \\ &\cdots \times I_{N-1, x_1^\pm x_{2N-1}^\pm} \end{aligned} \quad (3)$$

where the *influence functions* \mathbf{I}_k are defined in [Appendix A](#), and are related to the bath spectral density, $J(\omega) = \pi \sum_k \lambda_k^2 \delta(\omega - \omega_k)$. For later use, we note that Eq. (2) can be simplified into

$$\langle x_{2N}^+ | \rho_N | x_{2N}^- \rangle = \sum_{x_0^\pm} (\mathbf{U}_N)_{x_{2N}^\pm x_0^\pm} \langle x_0^+ | \rho_0 | x_0^- \rangle, \quad (4)$$

where \mathbf{U}_N is the system propagator from $t = 0$ to $t = N\Delta t$. It is then straightforward to express \mathbf{U}_N in terms of $\{\mathbf{I}_k\}$.^{22–24,45}

The Nakajima-Zwanzig Equation. The Nakajima-Zwanzig equation is a time-non-local formulation of the formally exact GQME. Assuming the time-independence of \hat{H}_S , the discretized homogeneous Nakajima-Zwanzig equation takes the form

$$\rho_N = \mathbf{L} \rho_{N-1} + \Delta t^2 \sum_{m=1}^N \mathcal{K}_{N-m} \rho_{m-1}, \quad (5)$$

where $\mathbf{L} \equiv (\mathbf{1} - \frac{i}{\hbar} \mathcal{L}_S \Delta t)$ with $\mathcal{L}_S \bullet \equiv [\hat{H}_S, \bullet]$ being the bare system Liouvillian and \mathcal{K}_n is the discrete-time memory kernel at timestep n . To relate \mathcal{K}_N to $\{\mathbf{I}_k\}$, we inspect the reduced dynamics evolution operator \mathbf{U}_N as defined in Eq. (4),

$$\mathbf{U}_N = \mathbf{L} \mathbf{U}_{N-1} + \Delta t^2 \sum_{m=1}^N \mathcal{K}_{N-m} \mathbf{U}_{m-1}. \quad (6)$$

With this relation, one can obtain \mathcal{K}_N from the reduced propagators $\{\mathbf{U}_k\}$. We observe setting $N = 1$

yields $\mathcal{K}_0 = \frac{1}{\Delta t^2} (\mathbf{U}_1 - \mathbf{L})$, since \mathbf{U}_0 is the identity. The memory kernel, \mathcal{K}_0 , accounts for the deviation of the system dynamics from its pure dynamics (decoupled from the bath) within a time step. From setting $N = 2$, we get $\mathcal{K}_1 = \frac{1}{\Delta t^2} (\mathbf{U}_2 - \mathbf{U}_1 \mathbf{U}_1)$. This intuitively shows that \mathcal{K}_1 captures the effect of the bath that cannot be captured within \mathcal{K}_0 . Similarly, for $N = 3$, $\mathcal{K}_2 = \frac{1}{\Delta t^2} (\mathbf{U}_3 - \mathbf{U}_2 \mathbf{U}_1 - \mathbf{U}_1 \mathbf{U}_2 + \mathbf{U}_1 \mathbf{U}_1 \mathbf{U}_1)$. This set of equations shows similarity to cumulant expansions widely used in the context of many-body physics and electronic structure theory.^{46,47} Instead of dealing with higher-order N -body expectation values, we deal with higher-order N -time memory kernel in this context. The N -time memory kernel \mathcal{K}_N is the N -th order cumulant in the cumulant expansion of the system operator. Unsurprisingly, these recursive relations lead to diagrammatic expansions commonly found in cumulant expansions⁴⁶ as shown in Fig. 1 panel (b).

Main results. Using this cumulant generation of \mathcal{K}_N and by expressing $\{\mathbf{U}_k\}$ in terms of $\{\mathbf{I}_k\}$, we obtain a direct relationship between \mathcal{K}_N and $\{\mathbf{I}_k\}_{k=0}^N$. Specifically, we have

$$\mathcal{K}_{0,ik} = \frac{1}{\Delta t^2} \left[\sum_j G_{ij} I_{0,j} G_{jk} - L_{ik} \right] \quad (7)$$

$$\mathcal{K}_{1,im} = \frac{1}{\Delta t^2} \sum_{jk} G_{ij} I_{0,j} F_{jk} \tilde{I}_{1,jk} I_{0,k} G_{km} \quad (8)$$

$$\begin{aligned} \mathcal{K}_{2,ip} &= \frac{1}{\Delta t^2} \sum_{jkn} G_{ij} F_{jk} F_{kn} (\tilde{I}_{2,jn} I_{1,jk} I_{1,kn} \\ &+ \tilde{I}_{1,jk} \tilde{I}_{1,kn}) I_{0,j} I_{0,k} I_{0,n} G_{np} \end{aligned} \quad (9)$$

$$\begin{aligned} \mathcal{K}_{3,il} &= \frac{1}{\Delta t^2} \sum_{jknlp} G_{ij} F_{jk} F_{kn} F_{np} I_{0,j} I_{0,k} I_{0,n} I_{0,p} G_{pl} \\ &\left\{ \tilde{I}_{3,jp} I_{2,jn} I_{2,kp} I_{1,jk} I_{1,kn} I_{1,np} \right. \\ &+ I_{1,kn} (\tilde{I}_{2,jn} \tilde{I}_{2,kp} I_{1,jk} I_{1,np} + \tilde{I}_{2,kp} \tilde{I}_{1,jk} I_{1,np} \\ &\left. + \tilde{I}_{2,jn} \tilde{I}_{1,np} I_{1,jk}) + \tilde{I}_{1,jk} \tilde{I}_{1,kn} \tilde{I}_{1,np} \right\} \end{aligned} \quad (10)$$

⋮

where we define $\mathbf{F} = \mathbf{G}\mathbf{G}$ (bold-face for denoting matrices) and $\tilde{I}_{k,ij} = I_{k,ij} - 1$. In [Appendix B](#), we present a general algorithm for calculating higher-order memory kernels, which is critical due to their nontrivial structure when expressed in terms of \mathbf{I} and $\tilde{\mathbf{I}}$. This series of equations is the main result of this work, showing explicitly how \mathcal{K}_N is constructed in terms of influence functions from \mathbf{I}_0 to \mathbf{I}_N . The computational effort of computing \mathcal{K}_N can be easily seen from this construction. We sum over an additional time index for each time step. This gives a computational cost that scales exponentially in time, $\mathcal{O}(N_{\text{dim}}^2 N)$ where N_{dim} is the dimension of the system Hilbert space.

It can be inferred from Eqs. (8) to (10) that each term in \mathcal{K}_N is represented uniquely by each Dyck path^{48–50} of order N . Hence, one can construct \mathcal{K}_N by generating the

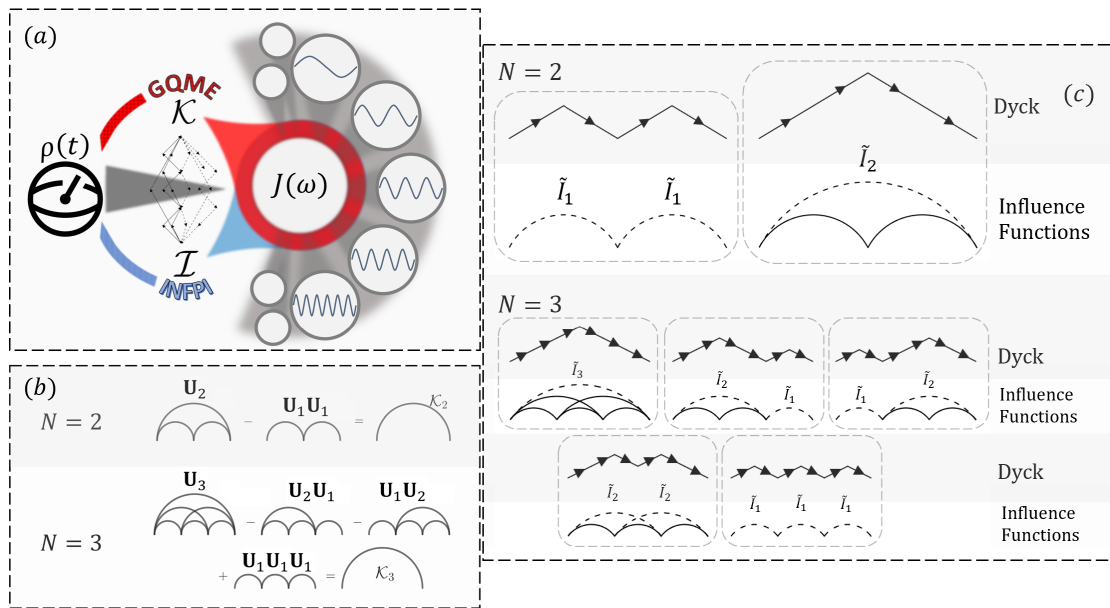


FIG. 1. **Unification of open quantum dynamics framework.** Panel (a): An open quantum system, where the environment is characterized by the spectral density $J(\omega)$, can be described with the Generalized Quantum Master Equation (GQME) and the Influence Functional Path Integral (INFPI). The former distills environmental correlations through the memory kernels \mathcal{K} while the latter through the influence functionals \mathcal{I} . In this work, we show both are related through Dyck Paths, and that furthermore we can use the Dyck construction for extracting $J(\omega)$ by simply knowing how the quantum system evolves. Panel (b): Cumulant expansion of memory kernel. Examples through Eq. (6) for $N = 2$ and $N = 3$. Solid arcs of diameter k filled with all possible arcs of diameters smaller than k denote propagator \mathcal{U}_k . Panel (c): Dyck path diagrams. Examples for $N = 2$ and $N = 3$ and their corresponding influence function diagrams, which composes \mathcal{K}_2 and \mathcal{K}_3 respectively. Solid lines denote influence functions \mathbf{I} and dashed line denote $\tilde{\mathbf{I}}$.

respective set of Dyck paths and associating each path with a tensor contraction of influence functions. This is illustrated in Fig. 1 panel (c) and further detailed in Appendix B. This observation reveals some new properties of \mathcal{K}_N . First, the number of terms in \mathcal{K}_N is given by the N -th Catalan's number^{49,50} $C_N = \frac{1}{N+1} \binom{2N}{N}$ (i.e., \mathcal{K}_4 has 14 such terms, \mathcal{K}_5 has 42, then 132, 429, 1430, 4862, 16796, 58786, ...). We note that Catalan's number appeared in Ref. 45 when analyzing an approximate numerical INFPI method. See Appendix B for more information.

Scrutinizing the relationship of \mathcal{K} and \mathbf{I} , presented in Appendix B, further, we can observe how \mathcal{K} decays asymptotically. As is well-known, for typical condensed phase systems $I_{k,ij} \rightarrow 1$ for $k \rightarrow \infty$.^{20,51} Similarly, because $\tilde{I}_{k,ij} \ll 1$ for large k , those terms with larger multiplicities contribute less to \mathcal{K}_N and decay exponentially to zero as multiplicity grows. In fact, for condensed phase systems, the decay of \mathbf{I}_N and \mathcal{K}_N is often rapid, which motivated the development of approximate INFPI methods^{20-23,51} and other approximate GQME methods.⁵²⁻⁵⁵

With our new insight, one can look at approximate INFPI methods through the lens of the corresponding memory kernel content (and vice versa). As an example, we shall discuss the iterative quasiadiabatic path-integral methods.^{20,21,51} In these methods, $I_{k,ij}$ is set to unity

beyond a preset truncation length k_{\max} . For simplicity, let us consider $k_{\max} = 1$, and hence $I_{k,ij} = 1$ and $\tilde{I}_{k,ij} = 0$ for $k > k_{\max}$. We now inspect what this approximation entails for \mathcal{K}_N . First, no approximation is applied to \mathcal{K}_0 and \mathcal{K}_1 . Then, in \mathcal{K}_2 (Eq. (9)),

$$(\tilde{I}_{2,jn} I_{1,jk} I_{1,kn} + \tilde{I}_{1,jk} \tilde{I}_{1,kn}) \rightarrow \tilde{I}_{1,jk} \tilde{I}_{1,kn}. \quad (11)$$

Similarly, in \mathcal{K}_3 (Eq. (10)), the only surviving contribution is from $\tilde{I}_{1,jk} \tilde{I}_{1,kn} \tilde{I}_{1,np}$. We hope such a direct connection between approximate methods will inspire the development of more efficient and accurate methods.

The time-translational structure of the INFPI formulation and its Dyck-diagrammatic structure allow for a recursive deduction of \mathbf{I}_N from \mathcal{K}_N , which is the inverse map of Eqs. (8) to (10). We first observe that

$$\mathbf{I}_0 = \mathbf{G}^{-1}(\delta t^2 \mathcal{K}_0 + \mathbf{L})\mathbf{G}^{-1} \quad (12)$$

where we obtained \mathbf{I}_0 from \mathcal{K}_0 . One can then show that

$$I_{1,jk} = 1 + \Delta t^2 \frac{(\mathbf{G}^{-1} \mathcal{K}_1 \mathbf{G}^{-1})_{jk}}{F_{jk} I_{0,j} I_{0,k}}. \quad (13)$$

using \mathcal{K}_1 and \mathbf{I}_0 . Similarly, inspecting the expression for \mathcal{K}_2 gives us

$$I_{2,jn} = 1 + \left[\Delta t^2 (\mathbf{G}^{-1} \mathcal{K}_2 \mathbf{G}^{-1})_{jn} \right]$$

$$\frac{-\sum_k F_{jk} F_{kn} \tilde{I}_{1,jk} \tilde{I}_{1,kn} I_{0,j} I_{0,k} I_{0,n}}{\sum_k F_{jk} F_{kn} I_{1,jk} I_{1,kn} I_{0,j} I_{0,k} I_{0,n}}, \quad (14)$$

where $\tilde{I}_{1,jk} = I_{1,jk} - 1$ as well as $I_{0,i}$ are obtained from the previous two relations.

In [Appendix C](#), we present a general recursive procedure using the Dyck paths and how to obtain the bath spectral density from I_k . As a result, we achieve the following mapping from left to right,

$$\rho \rightarrow \mathbf{U} \rightarrow \mathcal{K} \rightarrow \mathbf{I} \rightarrow J(\omega). \quad (15)$$

A remarkable outcome of this analysis is that one can completely characterize the environment (i.e., $J(\omega)$), by inspecting the reduced system dynamics. Such a tool is powerful in engineering quantum systems in experiments where we have access to only the reduced system Hamiltonian and reduced system dynamics, but lack information about the environment. Furthermore, this approach provides an alternative to quantum noise spectroscopy^{56,57}. This type of Hamiltonian learning with access only to subsystem observables has been achieved for other simpler Hamiltonians,^{58,59} but to our knowledge, for the Hamiltonian considered here, our work is the first to show this inverse map.

Note that the expression Eq. (13) can become ill-defined when \mathbf{F} is diagonal. This occurs when \hat{H}_S is diagonal and commutes with \hat{H}_{env} , constituting a purely dephasing dynamics. In that case, the reduced system dynamics is governed only by the diagonal elements of \mathbf{I} , and similarly \mathcal{K} is diagonal, as clearly seen in our Dyck path construction. As a result, the map $\mathcal{K} \leftrightarrow \mathbf{I}$ is no longer bijective in that we cannot obtain off-diagonal elements of \mathbf{I} . Regardless, one can still extract $J(\omega)$ using only the diagonal elements of \mathbf{I} via inverse cosine transform (see [Appendix C](#)). One may worry Eq. (14) could also become ill-conditioned when its denominator vanishes, but \hat{H}_S is not diagonal. If that were the case, the propagator \mathbf{U}_2 would become zero. Therefore, this condition cannot be satisfied in general.

Generalization to Driven Systems. While analysis up to this point considered general time-independent systems, in many scenarios, e.g., of biological or engineering relevance, particularly for quantum control applications⁶⁰, a time-dependent description of the system is necessary. In such cases, \mathcal{K} loses its time-translational properties and should depend on two times. Consequently, Eq. (6) cannot be applied. To overcome this, we factorize $\mathcal{K}_{N+s,s}$ into time-dependent and time-independent parts (see [Appendix D](#) for more details). This can be achieved straightforwardly, as follows: one observes upon the inclusion of time-dependence in \hat{H}_S , the terms that are affected in \mathcal{K}_N , Eqs. (7) to (10), are only the bare system propagators \mathbf{G} and \mathbf{F} . We define the remainder as tensors with N number of indices, $T_{N;x_{s+2},x_{s+4},\dots,x_{s+2N}}$, which includes all the influence of the bath between N time steps. These tensors only need to be computed once and reused for a later time. Then,

one builds the kernels via tensor contraction over two tensors,

$$\mathcal{K}_{N+s,s;x_{s+2N+2},x_s} = \frac{1}{\Delta t^2} \sum_{\bullet} P_{x_s,\bullet,x_{2N+2}}^{N+1+s,s} T_{N;\bullet}, \quad (16)$$

where \bullet denotes indices, x_{s+2}, \dots, x_{s+2N} , and the tensor $P_{x_s,\bullet,x_{2N+2}}^{N+1+s,s}$ encapsulates the time-dependence of the system Hamiltonian and is constructed only out of bare system propagators. The tensor, $T_{N;\bullet}$, then consists only of influence functions, up to \mathbf{I}_N . The construction of these tensors is straightforward with $T_{N;\bullet}$ following the Dyck path construction presented for time-independent system dynamics. Some relevant numerical results for open, driven system dynamics are presented in [Appendix D](#).

Numerical results. The spin-boson model is an archetypal model for studying open quantum systems.⁶¹ The model comprises a two-level system coupled linearly to a bath of harmonic oscillators. Hence, it and its generalizations have been used to understand various quantum phenomena: transport, chemical reactions, diode effect, and phase transitions.⁶² While the construction of \mathcal{K}_N discussed above is applicable to a generic system linearly coupled to a harmonic bath, we numerically verify our findings within the spin-boson model. Specifically, we now use $\hat{H}_S = \epsilon\sigma_z + \Delta\sigma_x$, coupled via σ_z to a harmonic bath with spectral density ($\omega \geq 0$)⁶¹

$$J(\omega) = \pi \sum_k \lambda_k^2 \delta(\omega - \omega_k) = \frac{\xi\pi}{2} \frac{\omega^s}{\omega_c^{s-1}} e^{-\omega/\omega_c}, \quad (17)$$

where $J(-\omega) = -J(\omega)$, ξ is the Kondo parameter, and s is the Ohmicity. All reference calculations were performed using the HEOM method.^{31,63,64} Details of the HEOM implementation used here are provided in [Appendix E](#).

In [Fig. 2](#), we investigate a series of spin-boson models corresponding to weak and intermediate coupling to an Ohmic environment ($s = 1$) as well as strong coupling to a subohmic environment ($s = 0.5$). In panels (a) and (b), we observe that the decay of $\tilde{\mathbf{I}}_N$ is rapid for the Ohmic cases. This translates to a similarly rapid decay for the respective \mathcal{K}_N , although one can see that both \tilde{I}_N and \mathcal{K}_N are overall scaled larger in the strong coupling regime. This is to be contrasted with the results for the strongly coupled subohmic environment shown in panel (c). The decay of the $\tilde{\mathbf{I}}_N$ is slow, accompanied by a similarly slow decay of \mathcal{K}_N . Interestingly, the rates by which both $\tilde{\mathbf{I}}_N$ and \mathcal{K}_N decay are similar. We also see perfect agreement between \mathcal{K}_N constructed from our Dyck diagrammatic method and those obtained by numerically post-processing exact trajectories via the transfer tensor method.⁴¹ Lastly, we construct $\tilde{\mathbf{I}}_N$ from \mathcal{K}_N up to $N = 16$ as exemplified in Eqs. (13) and (14) and observe perfect agreement between our $\tilde{\mathbf{I}}_N$ and those computed from its known analytic formula.

We note that the term with $\tilde{\mathbf{I}}_N$ (multiplicity of 1) contributes the most to the memory kernel, \mathcal{K}_N for all pa-

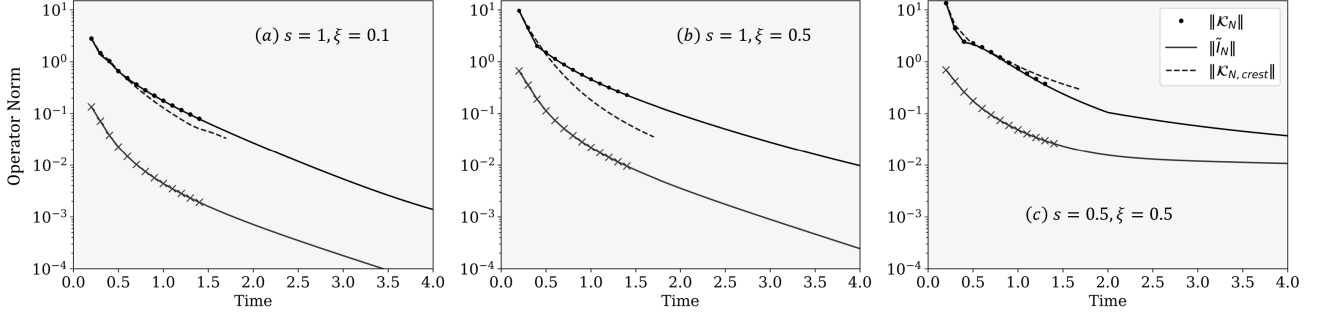


FIG. 2. **Verification of the Dyck construction.** Operator norm of $\tilde{\mathcal{I}}_N$ (Light) and \mathcal{K}_N (Dark) as a function of $N\Delta t$. Lines denote $\tilde{\mathcal{I}}_N$ computed from analytic expressions and \mathcal{K}_N from post-processing exact numerical results via the transfer tensor method.⁴¹ Circles denote \mathcal{K}_N from the Dyck diagrammatic method, and crosses are $\tilde{\mathcal{I}}_N$ obtained via the inverse map discussed in Eqs. (13) and (14). Dashed lines denote the operator norm of the crest term of \mathcal{K}_N (the Dyck path diagram with the highest height). Parameters used are: $\Delta = 1$ (other parameters are expressed relative to Δ), $\epsilon = 0$, $\beta = 5$, $\Delta t = 0.1$, $\omega_c = 7.5$, and $\xi = 0.1$ and $s = 1$ (panel (a)),

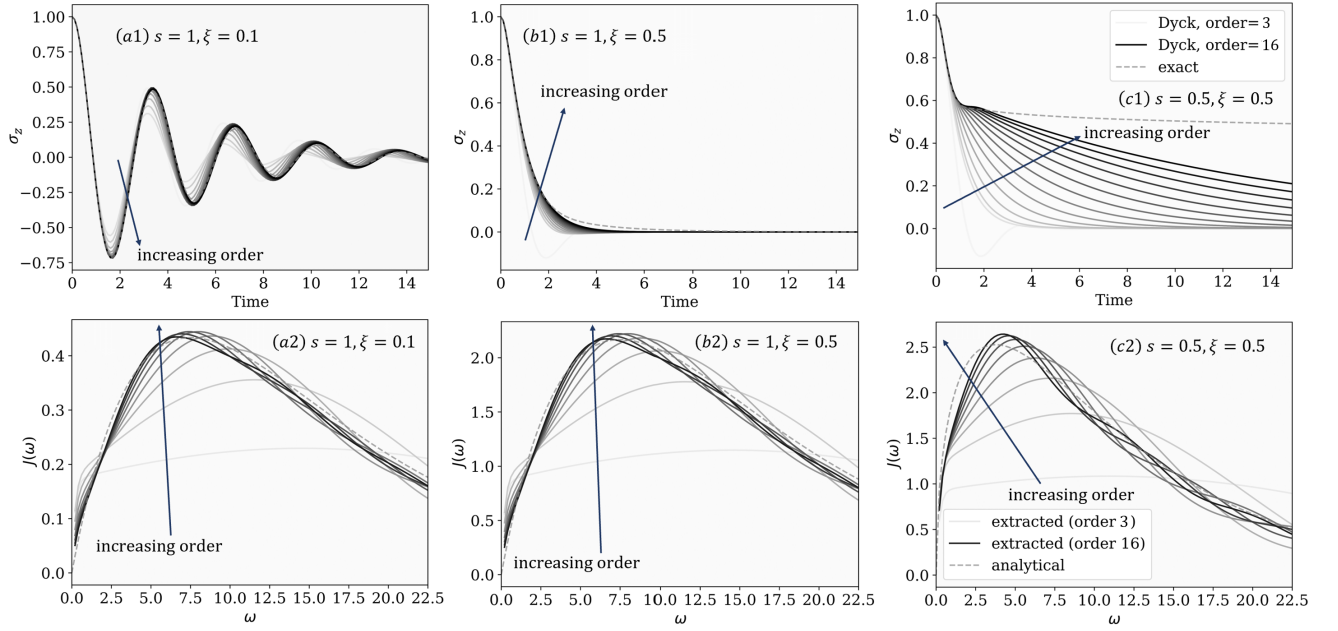


FIG. 3. **Dynamics of spin-boson model with truncated Dyck paths.** Panels (a1), (b1), and (c1): Magnetization ($\langle \sigma_z(t) \rangle$) dynamics predicted using \mathcal{K} constructed via Dyck diagrams with increasing truncation orders (from light to darker colors) compared to exact results (see Appendix F). Panels (a2), (b2), and (c2): Bath spectral densities extracted through the Dyck diagrammatic method with increasing truncation order (from white to black colors) compared to exact spectral densities (dashed), see Appendix C for more details. These results come from numerically exact trajectories, initiated from linearly independent initial states $\rho_1(0) = \frac{1}{2}(\mathbf{1} + \sigma_z)$, $\rho_2(0) = \frac{1}{2}(\mathbf{1} - \sigma_z)$, $\rho_3(0) = \frac{1}{2}(\mathbf{1} + \sigma_x)$, $\rho_4(0) = \frac{1}{2}(\mathbf{1} + \sigma_x + \sigma_y + \sigma_z)$. Parameters used are: $\Delta = 1$ (other parameters are expressed relative to Δ), $\epsilon = 0$, $\beta = 5$, $\Delta t = 0.1$ (panels (a1), (b1), and (c1)) or $\Delta t = 0.05$ (Panels (a2), (b2), and (c2)), $\omega_c = 7.5$, and $\xi = 0.1$ and $s = 1$ (panels (a1) and (a2)), $\xi = 0.5$ and $s = 1$ (panels (b1) and (b2)), or $\xi = 0.5$ and $s = 0.5$ (panels (c1) and (c2)).

rameters considered in our work. We refer to this term as the “crest” term, which corresponds to the Dyck path that goes straight to the top and down straight to the bottom, having the tallest height. We see a small difference between the crest term norm and the full memory kernel norm in Fig. 2, indicating that the memory kernel is dominated by the crest term. Since the decay of $\tilde{\mathcal{I}}_N$ is directly related to the decay of the bath correlation func-

tion, one can also make connections between the memory kernel decay and the bath correlation function decay. Nonetheless, for a stronger system-bath coupling (e.g., Fig. 2 (b)) and for cases with a long-lived memory (e.g., Fig. 2 (c)), terms other than the crest term contribute non-negligibly, making general analysis of the memory kernel decay challenging.

The cost to numerically compute \mathcal{K}_N scales exponen-

tially with N . Nevertheless, it is possible to exploit the decay of $\hat{\mathbf{I}}_N$, which is rapid for some environments, e.g., ohmic baths, in turn signifying the decay behavior of \mathcal{K}_N . This allows truncating the summation in Eq. (5), enabling dynamical propagation to long times (with linear costs in time) as usually done in small matrix path integral methods^{22,23} and GQME⁴¹ methods. We show in panels (a1) and (b1) of Fig. (3) that this procedure applied to a problem with a rapidly decaying \mathcal{K}_N quickly converges to the exact value with a reasonably low-order. On the other hand, for environments with slowly decaying $\hat{\mathbf{I}}_N$, the truncation scheme struggles to work effectively. For a strongly coupled subohmic environment, as shown in Fig. (3) panel (c1), one would need truncation orders beyond current computational capabilities (of about 16) to converge to the exact value. Nonetheless, this illustrates that our direct construction of \mathcal{K}_N can recover exact dynamics if sufficiently high-order is used. Furthermore, the construction is non-perturbative and can be applied to strong coupling problems.

Finally, in Fig. (3) panels (a2), (b2), and (c2), we show the extraction of spectral densities $J(\omega)$ for three distinct environments. The extracted $J(\omega)$ converges to the analytical value as we obtain the influence functions to higher orders. This shows that we can indeed invert the reduced system dynamics to obtain $J(\omega)$ given the knowledge of the system Hamiltonian, which ultimately characterizes the entire system-bath Hamiltonian. Nonetheless, the accuracy of the resulting $J(\omega)$ depends on the highest order of \mathbf{I}_k we can numerically extract. The cost of extracting \mathbf{I}_k scales exponentially in k without approximations, so there is naturally a limit to the precision of $J(\omega)$ in practice. Furthermore, we show how this procedure can extract highly structured spectral densities as well in Section Appendix F and Fig. 11. New opportunities await in using approximately inverted \mathbf{I}_k and quantifying the

error in the resulting $J(\omega)$.

Conclusion. In this Article, we provide analytical analysis and numerical evidence that show complete equivalence between the memory kernel (\mathcal{K}) in the GQME formalism and the influence function (\mathbf{I}) used in INFPI. Our analysis is applicable to a general (driven) system interacting with a harmonic bath via linear coupling. Furthermore, we presented a general, non-perturbative algorithm based on a diagrammatic analysis to construct \mathcal{K} exactly from the influence functions. Unlike available approaches, our direct construction of \mathcal{K} does not require any projection-free trajectories input. Furthermore, we showed that one can extract the bath spectral density from the reduced system dynamics with the knowledge of the reduced system Hamiltonian \hat{H}_S . We believe that this unified framework for studying non-Markovian dynamics will facilitate the development of new analytical and numerical methods that combine the strengths of both GQME and INFPI.

Acknowledgements. F.I. and J.L. were supported by Harvard University's startup funds. L.P.L acknowledges the support of the Engineering and Physical Sciences Research Council [grant EP/Y005090/1]. We thank Nathan Ng, David Reichman, Dvira Segal, and Jonathan Keeling for stimulating discussions, Tom O'Brien for discussions on Hamiltonian learning, and Hieu Dinh for providing a code to generate the Dyck path. Computations were carried out partly on the FASRC cluster supported by the FAS Division of Science Research Computing Group at Harvard University. This work also used the Delta system at the National Center for Supercomputing Applications through allocation CHE230078 from the Advanced Cyberinfrastructure Coordination Ecosystem: Services & Support (ACCESS) program, which is supported by National Science Foundation grants #2138259, #2138286, #2138307, #2137603, and #2138296.

* joonholee@g.harvard.edu

¹ H.-P. Breuer and F. Petruccione, *The theory of open quantum systems* (Oxford University Press, USA, 2002).

² T. V. Shahbazyan, Phys. Rev. B **105**, 245411 (2022), URL <https://link.aps.org/doi/10.1103/PhysRevB.105.245411>.

³ R. Finsterhölzl, M. Katzer, and A. Carmele, Phys. Rev. B **102**, 174309 (2020), URL <https://link.aps.org/doi/10.1103/PhysRevB.102.174309>.

⁴ S. Gröblacher, A. Trubarov, N. Prigge, G. D. Cole, M. Aspelmeyer, and J. Eisert, Nature Communications **6**, 7606 (2015), ISSN 2041-1723, URL <https://doi.org/10.1038/ncomms8606>.

⁵ A. Ivanov and H.-P. Breuer, Phys. Rev. A **92**, 032113 (2015), URL <https://link.aps.org/doi/10.1103/PhysRevA.92.032113>.

⁶ A. W. Chin, S. F. Huelga, and M. B. Plenio, Philosophical Transactions of the Royal Society A: Mathematical, Physical and Engineering Sciences **370**, 3638 (2012).

⁷ A. Ishizaki and G. R. Fleming, The Journal

of Chemical Physics **130**, 234111 (2009), ISSN 0021-9606, https://pubs.aip.org/aip/jcp/article-pdf/doi/10.1063/1.3155372/13131430/234111_1_online.pdf, URL <https://doi.org/10.1063/1.3155372>.

⁸ G. Spaventa, S. F. Huelga, and M. B. Plenio, Phys. Rev. A **105**, 012420 (2022), URL <https://link.aps.org/doi/10.1103/PhysRevA.105.012420>.

⁹ G. Andersson, B. Suri, L. Guo, T. Aref, and P. Delsing, Nature Physics **15**, 1123 (2019), ISSN 1745-2481, URL <https://doi.org/10.1038/s41567-019-0605-6>.

¹⁰ C.-F. Li, J.-S. Tang, Y.-L. Li, and G.-C. Guo, Phys. Rev. A **83**, 064102 (2011), URL <https://link.aps.org/doi/10.1103/PhysRevA.83.064102>.

¹¹ A. Smirne, D. Brivio, S. Cialdi, B. Vacchini, and M. G. A. Paris, Phys. Rev. A **84**, 032112 (2011), URL <https://link.aps.org/doi/10.1103/PhysRevA.84.032112>.

¹² A. Ask and G. Johansson, Phys. Rev. Lett. **128**, 083603 (2022), URL <https://link.aps.org/doi/10.1103/PhysRevLett.128.083603>.

¹³ J. Naikoo, S. Dutta, and S. Banerjee, Phys. Rev. A

- 99, 042128 (2019), URL <https://link.aps.org/doi/10.1103/PhysRevA.99.042128>.
- ¹⁴ B. Bylicka, D. Chruściński, and S. Maniscalco, *Scientific Reports* **4**, 5720 (2014), ISSN 2045-2322, URL <https://doi.org/10.1038/srep05720>.
- ¹⁵ B. Bylicka, D. Chruściński, and S. Maniscalco, *Non-markovianity as a resource for quantum technologies* (2013), 1301.2585.
- ¹⁶ H.-P. Breuer, E.-M. Laine, J. Piilo, and B. Vacchini, *Rev. Mod. Phys.* **88**, 021002 (2016), URL <https://link.aps.org/doi/10.1103/RevModPhys.88.021002>.
- ¹⁷ Y. Tanimura, *J. Chem. Phys.* **153** (2020), ISSN 0021-9606.
- ¹⁸ A. Strathearn, P. Kirton, D. Kilda, J. Keeling, and B. W. Lovett, *Nature Communications* **9**, 3322 (2018), ISSN 2041-1723, URL <https://doi.org/10.1038/s41467-018-05617-3>.
- ¹⁹ R. P. Feynman and F. L. Vernon, *Annals of Physics* **24**, 118 (1963), ISSN 0003-4916, URL <https://www.sciencedirect.com/science/article/pii/000349166390068X>.
- ²⁰ N. Makri and D. E. Makarov, *The Journal of Chemical Physics* **102**, 4611 (1995).
- ²¹ D. E. Makarov and N. Makri, *Chemical Physics Letters* **221**, 482 (1994).
- ²² N. Makri, *Journal of Chemical Theory and Computation* **17**, 1 (2021).
- ²³ N. Makri, *The Journal of Chemical Physics* **152**, 041104 (2020).
- ²⁴ S. Kundu and N. Makri, *The Journal of Chemical Physics* **158**, 224801 (2023), ISSN 0021-9606, https://pubs.aip.org/aip/jcp/article-pdf/doi/10.1063/5.0151748/17987394/224801_1.5.0151748.pdf, URL <https://doi.org/10.1063/5.0151748>.
- ²⁵ D. Segal, D. R. Reichman, and A. J. Millis, *Phys. Rev. B* **76**, 195316 (2007), URL <https://link.aps.org/doi/10.1103/PhysRevB.76.195316>.
- ²⁶ M. Kilgour, B. K. Agarwalla, and D. Segal, *The Journal of Chemical Physics* **150**, 084111 (2019), ISSN 0021-9606, URL <https://doi.org/10.1063/1.5084949>.
- ²⁷ L. Simine and D. Segal, *The Journal of Chemical Physics* **138**, 214111 (2013), ISSN 0021-9606, URL <https://doi.org/10.1063/1.4808108>.
- ²⁸ N. Makri, *The Journal of Chemical Physics* **149**, 214108 (2018), ISSN 0021-9606, https://pubs.aip.org/aip/jcp/article-pdf/doi/10.1063/1.5058223/15551048/214108_1_online.pdf, URL <https://doi.org/10.1063/1.5058223>.
- ²⁹ R. Lambert and N. Makri, *The Journal of Chemical Physics* **137**, 22A552 (2012), ISSN 0021-9606, https://pubs.aip.org/aip/jcp/article-pdf/doi/10.1063/1.4767931/14007017/22a552_1_online.pdf, URL <https://doi.org/10.1063/1.4767931>.
- ³⁰ Y. Tanimura, *Journal of the Physical Society of Japan* **75**, 082001 (2006), <https://doi.org/10.1143/JPSJ.75.082001>, URL <https://doi.org/10.1143/JPSJ.75.082001>.
- ³¹ M. Xu, Y. Yan, Q. Shi, J. Ankerhold, and J. T. Stockburger, *Phys. Rev. Lett.* **129**, 230601 (2022), URL <https://link.aps.org/doi/10.1103/PhysRevLett.129.230601>.
- ³² G. E. Fux, D. Kilda, B. W. Lovett, and J. Keeling, *Phys. Rev. Res.* **5**, 033078 (2023), URL <https://link.aps.org/doi/10.1103/PhysRevResearch.5.033078>.
- ³³ V. Link, H.-H. Tu, and W. T. Strunz, *arXiv* (2023), 2307.01802.
- ³⁴ D. Gribben, D. M. Rouse, J. Iles-Smith, A. Strathearn, H. Maguire, P. Kirton, A. Nazir, E. M. Gauger, and B. W. Lovett, *PRX Quantum* **3**, 010321 (2022), URL <https://link.aps.org/doi/10.1103/PRXQuantum.3.010321>.
- ³⁵ H.-P. Breuer and F. Petruccione, *The Theory of Open Quantum Systems* (Oxford University Press, 2007), ISBN 0199213909.
- ³⁶ S. Nakajima, *Progress of Theoretical Physics* **20**, 948 (1958), ISSN 0033-068X, URL <https://doi.org/10.1143/PTP.20.948>.
- ³⁷ R. Zwanzig, *The Journal of Chemical Physics* **33**, 1338 (1960), ISSN 0021-9606, URL <https://doi.org/10.1063/1.1731409>.
- ³⁸ E. Mulvihill and E. Geva, *J. Phys. Chem. B* **125**, 9834 (2021), ISSN 1520-6106.
- ³⁹ Q. Shi and E. Geva, *The Journal of chemical physics* **119**, 12063 (2003).
- ⁴⁰ Q. Shi and E. Geva, *The Journal of chemical physics* **121**, 3393 (2004).
- ⁴¹ J. Cerrillo and J. Cao, *Phys. Rev. Lett.* **112**, 110401 (2014), URL <https://link.aps.org/doi/10.1103/PhysRevLett.112.110401>.
- ⁴² L. Kidon, H. Wang, M. Thoss, and E. Rabani, *J. Chem. Phys.* **149** (2018), ISSN 0021-9606.
- ⁴³ G. Cohen and E. Rabani, *Phys. Rev. B* **84**, 075150 (2011).
- ⁴⁴ L. Mühlbacher and E. Rabani, *Phys. Rev. Lett.* **100**, 176403 (2008).
- ⁴⁵ G. Wang and Z. Cai, *Tree-based implementation of the small matrix path integral for system-bath dynamics* (2022), 2207.11830.
- ⁴⁶ G. D. Mahan, *Many-particle physics* (Springer Science & Business Media, 2000).
- ⁴⁷ W. Kutzelnigg and D. Mukherjee, *J. Chem. Phys.* **110**, 2800 (1999), ISSN 0021-9606.
- ⁴⁸ R. Brualdi, *Introductory Combinatorics* (Pearson/Prentice Hall, 2010), ISBN 9780136020400, URL <https://books.google.com/books?id=FOAkPwAACAAJ>.
- ⁴⁹ R. P. Stanley, *Catalan Numbers* (Cambridge University Press, 2015).
- ⁵⁰ *The on-line encyclopedia of integer sequences, sequence a000108* (2010), URL <https://oeis.org/A000108>.
- ⁵¹ N. Makri and D. E. Makarov, *The Journal of Chemical Physics* **102**, 4600 (1995).
- ⁵² A. Montoya-Castillo and D. R. Reichman, *The Journal of Chemical Physics* **144**, 184104 (2016), ISSN 0021-9606, https://pubs.aip.org/aip/jcp/article-pdf/doi/10.1063/1.4948408/13820400/184104_1_online.pdf, URL <https://doi.org/10.1063/1.4948408>.
- ⁵³ E. Mulvihill and E. Geva, *The Journal of Physical Chemistry B* **125**, 9834 (2021), ISSN 1520-6106, publisher: American Chemical Society, URL <https://doi.org/10.1021/acs.jpcc.1c05719>.
- ⁵⁴ E. Mulvihill, X. Gao, Y. Liu, A. Schubert, B. D. Dunietz, and E. Geva, *The Journal of Chemical Physics* **151**, 074103 (2019), ISSN 0021-9606, https://pubs.aip.org/aip/jcp/article-pdf/doi/10.1063/1.5110891/15562688/074103_1_online.pdf, URL <https://doi.org/10.1063/1.5110891>.
- ⁵⁵ A. Kelly, A. Montoya-Castillo, L. Wang, and T. E. Markland, *J. Chem. Phys.* **144** (2016), ISSN 0021-9606.
- ⁵⁶ C. L. Degen, F. Reinhard, and P. Cappellaro, *Rev. Mod. Phys.* **89**, 035002 (2017), URL <https://link.aps.org/doi/10.1103/RevModPhys.89.035002>.
- ⁵⁷ Y. Sung, A. Vepsäläinen, J. Braumüller, F. Yan, J. I.-J. Wang, M. Kjaergaard, R. Winik, P. Krantz, A. Bengts-

- son, A. J. Melville, et al., *Nature communications* **12**, 967 (2021).
- ⁵⁸ D. Burgarth, K. Maruyama, and F. Nori, *New J. Phys.* **13**, 013019 (2011), ISSN 1367-2630.
- ⁵⁹ C. Di Franco, M. Paternostro, and M. S. Kim, *Phys. Rev. Lett.* **102**, 187203 (2009).
- ⁶⁰ W.-L. Ma, S. Puri, R. J. Schoelkopf, M. H. Devoret, S. Girvin, and L. Jiang, *Science Bulletin* **66**, 1789 (2021), ISSN 2095-9273, URL <https://www.sciencedirect.com/science/article/pii/S2095927321004011>.
- ⁶¹ A. J. Leggett, S. Chakravarty, A. T. Dorsey, M. P. A. Fisher, A. Garg, and W. Zwerger, *Rev. Mod. Phys.* **59**, 1 (1987), URL <https://link.aps.org/doi/10.1103/RevModPhys.59.1>.
- ⁶² A. Nitzan, *Chemical Dynamics in Condensed Phases: Relaxation, Transfer, and Reactions in Condensed Molecular Systems* (New York: Oxford University Press, 2006).
- ⁶³ Y. Tanimura and R. Kubo, *J. Phys. Soc. Jpn.* **58**, 101 (1989).
- ⁶⁴ Y. Tanimura, *J. Chem. Phys.* **153**, 020901 (2020).
- ⁶⁵ N. Vilenkin, *Combinatorics [by] N. Ya. Vilenkin* (Academic Press, 1971), URL <https://books.google.com/books?id=MnNFNQAACAAJ>.
- ⁶⁶ A. Bernini, I. Fanti, and E. Grazzini, *An exhaustive generation algorithm for catalan objects and others* (2007), math/0612127.
- ⁶⁷ C. Neri, *A loopless and branchless o(1) algorithm to generate the next dyck word* (2018), 1602.06426.
- ⁶⁸ E. Deutsch and L. Shapiro, *Discrete Mathematics* **241**, 241 (2001), ISSN 0012-365X, selected Papers in honor of Helge Tverberg, URL <https://www.sciencedirect.com/science/article/pii/S0012365X01001212>.
- ⁶⁹ Y. Sun, *Discrete Mathematics* **287**, 177 (2004), ISSN 0012-365X, URL <https://www.sciencedirect.com/science/article/pii/S0012365X04003036>.
- ⁷⁰ OEIS Foundation Inc., *The On-Line Encyclopedia of Integer Sequences* (2023), published electronically at <http://oeis.org>.
- ⁷¹ N. Makri, *The Journal of Physical Chemistry A* **125**, 10500 (2021), pMID: 34812645, <https://doi.org/10.1021/acs.jpca.1c08230>, URL <https://doi.org/10.1021/acs.jpca.1c08230>.
- ⁷² Y. Nakatsukasa, O. Sète, and L. N. Trefethen, *SIAM Journal on Scientific Computing* **40**, A1494 (2018), <https://doi.org/10.1137/16M1106122>, URL <https://doi.org/10.1137/16M1106122>.
- ⁷³ Q. Shi, Y. Xu, Y. Yan, and M. Xu, *The Journal of Chemical Physics* **148**, 174102 (2018), ISSN 0021-9606, https://pubs.aip.org/aip/jcp/article-pdf/doi/10.1063/1.5026753/15539991/174102.1_online.pdf, URL <https://doi.org/10.1063/1.5026753>.
- ⁷⁴ E. Mangaud, A. Jaouadi, A. Chin, and M. Desouter-Lecomte, *The European Physical Journal Special Topics* **232**, 1847 (2023), ISSN 1951-6401, URL <https://doi.org/10.1140/epjs/s11734-023-00919-0>.
- ⁷⁵ L. P. J. Lindoy, D.phil. thesis, Magdalen College, University of Oxford (2019), URL <https://ora.ox.ac.uk/objects/uuid:2d98ae52-9e1d-4c6d-a940-d8b9131e0275>.
- ⁷⁶ Y. Ke, *The Journal of Chemical Physics* **158**, 211102 (2023), ISSN 0021-9606, <https://pubs.aip.org/aip/jcp/article-pdf/doi/10.1063/5.0153870/18143581/211102.1.5.0153870.pdf>, URL <https://doi.org/10.1063/5.0153870>.
- ⁷⁷ D. Bauernfeind, M. Zingl, R. Triebel, M. Aichhorn, and H. G. Evertz, *Phys. Rev. X* **7**, 031013 (2017), URL <https://link.aps.org/doi/10.1103/PhysRevX.7.031013>.
- ⁷⁸ D. Bauernfeind, Phd thesis, Graz University of Technology (2018), URL https://online.tugraz.at/tug_online/wbAbs.showThesis?pThesisNr=63872&pOrgNr=37.

Appendix A. PATH INTEGRAL FORMULATION

A. Theory

We present a more detailed formulation of the influence-functional-based path-integral (INFPI) approaches. We consider the general Hamiltonian of a quantum system interacting with external degrees of freedom,

$$\hat{H} = \hat{H}_S + \hat{H}_B + \hat{H}_I, \quad (\text{A1})$$

where \hat{H}_S is the system Hamiltonian, $\hat{H}_B = \sum_k \omega_k \hat{b}_k^\dagger \hat{b}_k$, and $\hat{H}_I = \hat{S} \otimes \hat{B}$ where \hat{S} is a system operator and $\hat{B} = \sum_k \lambda_k (\hat{b}_k^\dagger + \hat{b}_k)$. The time evolution of the density matrix of the full system, $\rho_{\text{tot}}(t) \equiv |\psi(t)\rangle\langle\psi(t)|$ (pure state for simplicity, further assumed separable $\rho_{\text{tot}}(0) = \rho(0) \otimes \frac{\exp[-\beta\hat{H}_B]}{\text{Tr}\exp[-\beta\hat{H}_B]}$) follows

$$\rho_{\text{tot}}(t) = e^{-i\hat{H}t} \rho_{\text{tot}}(0) e^{i\hat{H}t}. \quad (\text{A2})$$

With the quasiadiabatic approximation, one may split the total Hamiltonian as (here $\hat{H}_{\text{env}} = \hat{H} - \hat{H}_S$)

$$e^{-i\hat{H}\Delta t} \rightarrow e^{-i\hat{H}_S\Delta t/2} e^{-i\hat{H}_{\text{env}}\Delta t} e^{-i\hat{H}_S\Delta t/2} + O(\Delta t^3). \quad (\text{A3})$$

With this identity we express the trotterized evolution as (summation over the paths implied)

$$\langle x_{2N}^+ | \rho_{\text{tot}}(t) | x_{2N}^- \rangle = \langle x_{2N}^+ | e^{-i\hat{H}_S\Delta t/2} e^{-i\hat{H}_{\text{env}}\Delta t} e^{-i\hat{H}_S\Delta t/2} | x_{2N-2}^+ \rangle$$

$$\cdots \langle x_0^+ | \rho_{\text{tot}}(0) | x_0^- \rangle \cdots \langle x_{2N-2}^- | e^{i\hat{H}_S \Delta t/2} e^{i\hat{H}_{\text{env}} \Delta t} e^{i\hat{H}_S \Delta t/2} | x_{2N}^- \rangle. \quad (\text{A4})$$

We work in the diagonal \hat{S} basis (note $\hat{H}_I = \hat{S} \otimes \hat{B}$ for some system operator \hat{S} and bath operator \hat{B}) and insert resolution-of-the-identity in between every $e^{\pm i\hat{H}_S \Delta t/2}$ and $e^{i\hat{H}_{\text{env}} \Delta t}$ to obtain

$$\langle x_{2N}^+ | \rho_{\text{tot}}(t) | x_{2N}^- \rangle = \langle x_{2N}^+ | e^{-i\hat{H}_S \Delta t/2} | x_{2N}^+ \rangle \langle x_{2N}^+ | e^{-i\hat{H}_{\text{env}} \Delta t} | x_{2N-2}^+ \rangle \langle x_{2N-2}^+ | e^{-i\hat{H}_S \Delta t/2} | x_{2N-2}^+ \rangle \cdots. \quad (\text{A5})$$

Since

$$\langle x_{2N}^+ | e^{-i\hat{H}_{\text{env}} \Delta t} | x_{2N-2}^+ \rangle \propto \delta_{x_{2N}^+, x_{2N-2}^+ \equiv x_{2N-1}^+}, \quad (\text{A6})$$

we therefore have

$$\langle x_{2N}^+ | \rho_{\text{tot}}(t) | x_{2N}^- \rangle = G_{x_{2N}^\pm x_{2N-1}^\pm} G_{x_{2N-1}^\pm x_{2N-2}^\pm} \cdots \langle x_0^+ | \rho(0) | x_0^- \rangle \text{Tr}_B [e^{-i\hat{H}_{\text{env}}(x_{2N-1}^+) \Delta t} \cdots \rho_B \cdots e^{i\hat{H}_{\text{env}}(x_{2N-1}^-) \Delta t}] \quad (\text{A7})$$

where $G_{x_m^\pm x_{m-1}^\pm} = \langle x_m^+ | e^{-i\hat{H}_S \Delta t/2} | x_{m-1}^+ \rangle \langle x_{m-1}^- | e^{i\hat{H}_S \Delta t/2} | x_m^- \rangle$.

When the density matrix is separable (as assumed earlier) and where \hat{H}_B is quadratic in bath operators (as we have and as assumed commonly) the influence functionals take a pairwise product form as shown in Eq. (3). For $k' \geq k$, influence functions are given as

$$I_{k'-k, x_k^\pm x_{k'}^\pm} = \exp\{-(x_k^+ - x_k^-)(\eta_{kk'} x_{k'}^+ - \eta_{kk'}^* x_{k'}^-)\}, \quad (\text{A8})$$

where

$$\eta_{kk'} = \frac{2}{\pi} \int_{-\infty}^{\infty} d\omega \left(\frac{J(\omega) \exp\{\beta \hbar \omega/2\}}{\omega^2 \sinh \beta \hbar \omega/2} \sin^2(\omega \Delta t/2) e^{-i\omega \Delta t(k-k')} \right), \quad (\text{A9})$$

$$\eta_{kk} = \frac{1}{2\pi} \int_{-\infty}^{\infty} d\omega \frac{J(\omega) \exp\{\beta \hbar \omega/2\}}{\omega^2 \sinh \beta \hbar \omega/2} (1 - e^{-i\omega \Delta t}). \quad (\text{A10})$$

We recall that

$$J(\omega) = \frac{\xi \pi}{2} \omega e^{-\omega/\omega_c} = \pi \sum_k \lambda_k^2 \delta(\omega - \omega_k). \quad (\text{A11})$$

Note that we can recover Eq. (A10) from Eq. (A9) by using $\sin^2(x/2) - \frac{1}{2}(1 - e^{-ix}) = -\frac{1}{2}i \sin x$ which is a purely imaginary and odd function.

If one writes the propagators in a more compact form (for $k > 0$)

$$\begin{aligned} U_{k, x_{2k}^\pm x_0^\pm} &= \sum_{x_{2k-1}^\pm} G_{x_{2k}^\pm x_{2k-1}^\pm} \sum_{x_1^\pm} \tilde{U}_{k-1, x_{2k-1}^\pm x_1^\pm} G_{x_1^\pm x_0^\pm}, \\ F_{x_{2k+1}^\pm x_{2k-1}^\pm} &= \sum_{x_{2k}^\pm} G_{x_{2k+1}^\pm x_{2k}^\pm} G_{x_{2k}^\pm x_{2k-1}^\pm}, \end{aligned} \quad (\text{A12})$$

the auxiliary propagators can be written as

$$\tilde{U}_{0, x_1^\pm x_1^\pm} = I_{0, x_1^\pm} \quad (\text{A13})$$

$$\begin{aligned} \tilde{U}_{1, x_3^\pm x_1^\pm} &= F_{x_3^\pm x_1^\pm} I_{1, x_3^\pm x_1^\pm} I_{0, x_3^\pm} I_{0, x_1^\pm} \\ &= \underbrace{F_{x_3^\pm x_1^\pm} I_{1, x_3^\pm x_1^\pm} I_{0, x_3^\pm}}_{M_{1, x_3^\pm x_1^\pm}} \tilde{U}_{0, x_1^\pm x_1^\pm} \end{aligned} \quad (\text{A14})$$

$$\begin{aligned} \tilde{U}_{2, x_5^\pm x_1^\pm} &= \sum_{x_3^\pm} F_{x_5^\pm x_3^\pm} F_{x_3^\pm x_1^\pm} I_{2, x_5^\pm x_1^\pm} I_{1, x_5^\pm x_3^\pm} I_{1, x_3^\pm x_1^\pm} I_{0, x_5^\pm} I_{0, x_3^\pm} I_{0, x_1^\pm} \\ &= \sum_{x_3^\pm} \underbrace{F_{x_5^\pm x_3^\pm} I_{1, x_5^\pm x_3^\pm} I_{0, x_5^\pm}}_{M_{1, x_5^\pm x_3^\pm}} \underbrace{F_{x_3^\pm x_1^\pm} I_{1, x_3^\pm x_1^\pm} I_{0, x_3^\pm} I_{0, x_1^\pm}}_{\tilde{U}_{1, x_3^\pm x_1^\pm}} \end{aligned}$$

$$+(I_{2,x_5^\pm x_1^\pm} - 1) \sum_{x_3^\pm} F_{x_5^\pm x_3^\pm} F_{x_3^\pm x_1^\pm} I_{1,x_5^\pm x_3^\pm} I_{1,x_3^\pm x_1^\pm} I_{0,x_5^\pm} I_{0,x_3^\pm} I_{0,x_1^\pm}, \quad (\text{A15})$$

where the underbraced M terms and the last line is analogous to the memory matrix in small matrix path integral (SMatPI) methods²²⁻²⁴ and the transfer tensors in the transfer tensor method (TTM)⁴¹, both of which can be cast into the memory kernels \mathcal{K} . However, crucial differences emerge here which makes Eqs. (A13) - (A15) *distinct* and cannot be obtained from SMatPI or TTM: (1) Here they are completely time-translationally invariant, while in SMatPI they are not, (2) Here $\mathbf{M}_1 \neq \mathbf{U}_1$ and therefore the analysis of TTM is not applicable. One may proceed as in the main text to recover the memory kernels \mathcal{K} from the propagators.

B. Explicit Correspondence with GQME

The Nakajima-Zwanzig (NZ) equation takes the form

$$\dot{\rho}(t) = -\frac{i}{\hbar} \mathcal{L} \rho(t) + \int_0^t d\tau \mathcal{K}(t, \tau) \rho(\tau) + \mathcal{I}(t). \quad (\text{A16})$$

In this work, the inhomogeneous term $\mathcal{I}(t)$ vanishes due to the factorized initial condition assumption $\rho_{\text{tot}}(0) = \rho(0) \otimes \rho_B$. The *discretized* form of the homogeneous NZ equation is (with $t = (N-1)\Delta t$)

$$\frac{\rho_N - \rho_{N-1}}{\Delta t} = -\frac{i}{\hbar} \mathcal{L}_s \rho_{N-1} + \sum_{m=1}^N \mathcal{K}_{N,m} \rho_m \Delta t. \quad (\text{A17})$$

By noting that $\rho_N = U_N \rho_0$ (where $\rho_N = \rho(N\Delta t)$) we get

$$\mathbf{U}_N = \mathbf{L} \mathbf{U}_{N-1} + \Delta t^2 \sum_{m=1}^N \mathcal{K}_{N,m} \mathbf{U}_{m-1}. \quad (\text{A18})$$

We then obtain \mathcal{K} in terms of I by matching each multiplier of \mathbf{U}_k recursively. For example, for $N=1$,

$$\frac{\rho_1 - \rho_0}{\Delta t} = -\frac{i}{\hbar} \mathcal{L}_s \rho_0 + \mathcal{K}_{1,1} \rho_0 \Delta t \quad (\text{A19})$$

so

$$\mathbf{U}_1 = \left(1 - \frac{i}{\hbar} \mathcal{L}_s \Delta t\right) + \mathcal{K}_{1,1} \Delta t^2, \quad (\text{A20})$$

that is,

$$(\mathcal{K}_{1,1})_{ik} = \frac{1}{\Delta t^2} \left[\sum_j G_{ij} I_j^0 G_{jk} + \left(\frac{i}{\hbar} \mathcal{L}_s \Delta t - 1\right)_{ik} \right]. \quad (\text{A21})$$

For $N=2$,

$$\frac{\rho_2 - \rho_1}{\Delta t} = -\frac{i}{\hbar} \mathcal{L}_s \rho_1 + [\mathcal{K}_{2,1} \rho_0 + \mathcal{K}_{2,2} \rho_1] \Delta t. \quad (\text{A22})$$

One observes that with the time-translational invariance of the memory kernels (i.e., valid if the system Hamiltonian does not have explicit time-dependence),

$$\mathcal{K}_{2,1} = \mathcal{K}_{3,2} \equiv \mathcal{K}_1. \quad (\text{A23})$$

We use this and make appropriate substitutions in our previous results. Then, we obtain

$$\mathcal{K}_1 \rho_0 = \frac{1}{\Delta t^2} [\mathbf{U}_2 - \mathbf{U}_1 \mathbf{U}_1] \rho_0. \quad (\text{A24})$$

Hence,

$$(\mathcal{K}_1)_{im} = \frac{1}{\Delta t^2} \left[\sum_j G_{ij} \sum_k F_{jk} I_{1,jk} I_{0,j} I_{0,k} G_{km} - \sum_j G_{ij} I_{0,j} \sum_k G_{jk} \sum_l G_{kl} I_{0,l} G_{lm} \right]. \quad (\text{A25})$$

Similarly, for $N = 3$,

$$\begin{aligned}\rho_3 &= \left(\mathbf{1} - \frac{i}{\hbar}\mathcal{L}_s\Delta t\right)\rho_2 + [\mathcal{K}_{3,1}\rho_0 + \mathcal{K}_{3,2}\rho_1 + \mathcal{K}_{3,3}\rho_2]\Delta t^2 \\ \mathbf{U}_3\rho_0 &= \left(\mathbf{1} - \frac{i}{\hbar}\mathcal{L}_s\Delta t\right)\mathbf{U}_2\rho_0 + [\mathcal{K}_{3,1} + \frac{1}{\Delta t^2}(\mathbf{U}_2 - \mathbf{U}_1\mathbf{U}_1)]\mathbf{U}_1 \\ &\quad + \frac{1}{\Delta t^2}\left(\frac{i}{\hbar}\mathcal{L}_s\Delta t - 1 + \mathbf{U}_1\right)\mathbf{U}_2\rho_0\Delta t^2.\end{aligned}\tag{A26}$$

One observes many terms again cancel, leaving

$$\mathcal{K}_2 = \frac{1}{\Delta t^2}\left[-\mathbf{U}_2\mathbf{U}_1 + \mathbf{U}_1\mathbf{U}_1\mathbf{U}_1 - \mathbf{U}_1\mathbf{U}_2 + \mathbf{U}_3\right].\tag{A27}$$

Making appropriate substitutions into \mathbf{U}_1 , \mathbf{U}_2 , and \mathbf{U}_3 ,

$$\begin{aligned}(\mathcal{K}_2)_{ip} &= \frac{1}{\Delta t^2}\left[-\sum_j G_{ij}I_{0,j}\sum_k F_{jk}I_{1,jk}I_{0,k}\sum_n K_{kn}I_{0,n}G_{np} + \sum_j G_{ij}I_{0,j}\sum_k F_{jk}I_{0,k}\sum_n F_{kn}I_{0,n}G_{np}\right. \\ &\quad \left.-\sum_j G_{ij}I_{0,j}\sum_k F_{jk}\sum_n F_{kn}I_{1,kn}I_{0,k}I_{0,n}G_{np} + \sum_{jkn} G_{ij}F_{jk}F_{kn}I_{2,jn}I_{1,jk}I_{1,kn}I_{0,j}I_{0,k}I_{0,n}G_{np}\right].\end{aligned}\tag{A28}$$

We again factorize as follows

$$I_{2,jn}I_{1,jk}I_{1,kn} = (I_{2,jn} - 1)I_{1,jk}I_{1,kn} + \underbrace{I_{1,jk} + I_{1,kn} - 1}_{\text{underbraced}} + (I_{1,jk} - 1)(I_{1,kn} - 1).\tag{A29}$$

The underbraced terms cancel with the first three terms in Eq. (A28) and we are left with

$$(\mathcal{K}_2)_{ip} = \sum_{jkn} G_{ij}F_{jk}F_{kn}[(I_{2,jn} - 1)I_{1,jk}I_{1,kn} + (I_{1,jk} - 1)(I_{1,kn} - 1)]I_{0,j}I_{0,k}I_{0,n}G_{np}.\tag{A30}$$

For $N = 4$,

$$\begin{aligned}\rho_4 &= \left(\mathbf{1} - \frac{i}{\hbar}\mathcal{L}_s\Delta t\right)\rho_3 + [\mathcal{K}_{4,1}\rho_0 + \mathcal{K}_{4,2}\rho_1 + \mathcal{K}_{4,3}\rho_2 + \mathcal{K}_{4,4}\rho_3]\Delta t^2 \\ \mathbf{U}_4\rho_0 &= \left(\mathbf{1} - \frac{i}{\hbar}\mathcal{L}_s\Delta t\right)\mathbf{U}_3\rho_0 + [\mathcal{K}_{4,1} + \mathcal{K}_2\mathbf{U}_1 + \frac{1}{\Delta t^2}(\mathbf{U}_2 - \mathbf{U}_1\mathbf{U}_1)]\mathbf{U}_2 \\ &\quad + \frac{1}{\Delta t^2}\left(\frac{i}{\hbar}\mathcal{L}_s\Delta t - 1 - \mathbf{U}_1\right)\mathbf{U}_3\rho_0\Delta t^2.\end{aligned}\tag{A31}$$

So,

$$\begin{aligned}(\mathcal{K}_3)_{il} &= \sum_{jknp} G_{ij}F_{jk}F_{kn}F_{np}[I_{3,jp}I_{2,jn}I_{2,kp}I_{1,jk}I_{1,kn}I_{1,np} + I_{1,jk} - 1 + I_{1,kn} - I_{2,jn}I_{1,jk}I_{1,kn} \\ &\quad - I_{1,jk}I_{1,np} + I_{1,np} - I_{2,kp}I_{1,kn}I_{1,np}]I_{0,j}I_{0,k}I_{0,n}I_{0,p}G_{pl}.\end{aligned}\tag{A32}$$

We factorize as follows

$$I_{3,jp}I_{2,jn}I_{2,kp}I_{1,jk}I_{1,kn}I_{1,np} = (I_{3,jp} - 1)I_{2,jn}I_{2,kp}I_{1,jk}I_{1,kn}I_{1,np} + I_{2,jn}I_{2,kp}I_{1,jk}I_{1,kn}I_{1,np}.\tag{A33}$$

For now notice that

$$\begin{aligned}I_{2,jn}I_{2,kp}I_{1,jk}I_{1,kn}I_{1,np} - I_{2,jn}I_{1,jk}I_{1,kn} - I_{2,kp}I_{1,kn}I_{1,np} &= I_{1,kn}(I_{2,jn}I_{2,kp}I_{1,jk}I_{1,np} - I_{2,jn}I_{1,jk} - I_{2,kp}I_{1,np}) \\ &= I_{1,kn}[(I_{2,jn} - 1)(I_{2,kp} - 1)I_{1,jk}I_{1,np} + I_{1,jk}I_{1,np} - (I_{2,jn} - 1)I_{1,jk} - I_{1,jk} - (I_{2,kp} - 1)I_{1,np} - I_{1,np}) \\ &\quad (I_{2,kp} - 1)I_{1,jk}I_{1,np} + (I_{2,jn} - 1)I_{1,jk}I_{1,np}]\end{aligned}\tag{A34}$$

because

$$\begin{aligned}I_{2,jn}I_{2,kp}I_{1,jk}I_{1,np} &= I_{2,kp}I_{1,jk}I_{1,np} + (I_{2,jn} - 1)I_{2,kp}I_{1,jk}I_{1,np} \\ &= (I_{2,kp} - 1)I_{1,jk}I_{1,np} + (I_{2,jn} - 1)I_{1,jk}I_{1,np} + I_{1,jk}I_{1,np}\end{aligned}$$

$$+(I_{2,jn} - 1)I_{2,kp}I_{1,jk}I_{1,np} + (I_{2,jn} - 1)(I_{2,kp} - 1)I_{1,jk}I_{1,np} \quad (\text{A35})$$

note there

$$\begin{aligned} & (I_{2,jn} - 1)(I_{2,kp} - 1)I_{1,jk}I_{1,np} + (I_{2,kp} - 1)I_{1,jk}I_{1,np} + (I_{2,jn} - 1)I_{1,jk}I_{1,np} - (I_{2,jn} - 1)I_{1,jk} - (I_{2,kp} - 1)I_{1,np} \\ = & (I_{2,jn} - 1)(I_{2,kp} - 1)I_{1,jk}I_{1,np} + (I_{2,kp} - 1)(I_{1,jk} - 1)I_{1,np} + (I_{2,jn} - 1)(I_{1,np} - 1)I_{1,jk} \end{aligned} \quad (\text{A36})$$

and also that

$$I_{1,kn}[I_{1,jk}I_{1,np} - I_{1,jk} - I_{1,np}] + I_{1,jk} - 1 + I_{1,kn} - I_{1,jk}I_{1,np} + I_{1,np} = (I_{1,jk} - 1)(I_{1,kn} - 1)(I_{1,np} - 1). \quad (\text{A37})$$

These resulting identities then group terms in Eq. (A32) to give Eq. (10) in the main text. Now for \mathcal{K}_4 (we use $\tilde{I}_{i,jk} = (I_{i,jk} - 1)$):

$$\begin{aligned} \mathcal{K}_{4,im} = & \frac{1}{\Delta t^2} \sum_{jknpl} G_{ij} F_{jk} F_{kn} F_{np} F_{pl} I_{0,j} I_{0,k} I_{0,n} I_{0,p} I_{0,l} G_{lm} \{ \\ & \tilde{I}_{4,jl} I_{1,jk} I_{2,jn} I_{3,jp} I_{1,kn} I_{2,kp} I_{3,kl} I_{1,np} I_{2,nl} I_{1,pl} \\ & + \tilde{I}_{3,jp} I_{1,jk} I_{2,jn} I_{1,kn} I_{2,kp} I_{1,np} \tilde{I}_{3,kl} I_{2,nl} I_{1,pl} + \tilde{I}_{3,jp} I_{1,jk} I_{2,jn} I_{1,kn} I_{2,kp} I_{1,np} \tilde{I}_{2,nl} I_{1,pl} \\ & + \tilde{I}_{3,jp} I_{1,jk} I_{2,jn} I_{1,kn} I_{2,kp} I_{1,np} \tilde{I}_{1,pl} + \tilde{I}_{2,jn} I_{1,jk} I_{1,kn} \tilde{I}_{3,kl} I_{2,kp} I_{1,np} I_{2,nl} I_{1,pl} + \tilde{I}_{2,jn} I_{1,jk} I_{1,kn} \tilde{I}_{2,kp} I_{1,np} \tilde{I}_{2,nl} I_{1,pl} \\ & + \tilde{I}_{2,jn} I_{1,jk} I_{1,kn} \tilde{I}_{2,kp} I_{1,np} \tilde{I}_{1,pl} + \tilde{I}_{2,jn} I_{1,jk} I_{1,kn} \tilde{I}_{2,nl} I_{1,np} I_{1,pl} + \tilde{I}_{2,jn} I_{1,jk} I_{1,kn} \tilde{I}_{1,np} \tilde{I}_{1,pl} \\ & + \tilde{I}_{1,jk} \tilde{I}_{3,kl} I_{1,kn} I_{2,kp} I_{1,np} I_{2,nl} I_{1,pl} + \tilde{I}_{1,jk} \tilde{I}_{2,kp} I_{1,kn} I_{1,np} \tilde{I}_{2,nl} I_{1,pl} + \tilde{I}_{1,jk} \tilde{I}_{2,kp} I_{1,kn} I_{1,np} \tilde{I}_{1,pl} \\ & + \tilde{I}_{1,jk} \tilde{I}_{1,kn} \tilde{I}_{2,nl} I_{1,np} I_{1,pl} + \tilde{I}_{1,jk} \tilde{I}_{1,kn} \tilde{I}_{1,np} \tilde{I}_{1,pl} \}. \end{aligned} \quad (\text{A38})$$

Evidently, the number of terms grows combinatorially with the number of timesteps N . In the next section, we devise a general scheme to build memory kernels at arbitrary time $N\Delta t$ based on Dyck diagrams.

Appendix B. NAKAJIMA-ZWANZIG DYCK-DIAGRAMMATIC FORMALISM

The structure of terms in \mathcal{K}_N via the decomposition through $\{\mathbf{I}_k\}$ has the following properties. The number of terms in \mathcal{K}_N is given by Catalan's numbers^{49,50} $C_N = \frac{1}{N+1} \binom{2N}{N}$, as was pointed out in Ref. 45. More importantly, the terms in \mathcal{K}_N are given by Dyck path diagrams^{49,50} (of which there are C_N paths). A Dyck path is a sequence of up-steps and down-steps that start and end on the x -axis but never go below. The order of a Dyck path is given by the number of up-steps, which must equal the number of down-steps. The study of Dyck paths is at the root of combinatorial mathematics⁶⁵, and algorithms already exist to generate all Dyck paths of any order.^{66,67} Alternatively, one can also generate all $P^R(N, k) = k^N$ (sometimes also called k -tuples) possible permutations (repetitions allowed, since here $k = 2$ accounting for up or down steps we then have $P^R(2, 2) = 4$, $P^R(4, 2) = 16$, $P^R(6, 2) = 64$, and so on) of \nearrow and \searrow and then filter (i.e., such path must have equal amounts of \nearrow and \searrow and furthermore at any point the path must not go below the x -axis and so on) for an order $2N$ Dyck path. To obtain the terms in \mathcal{K}_N from a particular Dyck path, we map a Dyck path into an influence functional diagram based on the following rules:

1. The Dyck path is made dashed.
2. Now one draws all possible triangles in each segment of a Dyck path, but none could be as tall as any dashed peak. This step is drawn in solid. A segment of a Dyck path is defined as the sub-path of a Dyck path which starts and ends at $x = 0$ (the full path itself is not counted). A peak is defined as the point at which an up-step meets a down-step, in that order.
3. If any dashed down path sequence does not reach $x = 0$, one continues to draw it until it does, this is with dashed lines.
4. One rounds the vertices.
5. Dashed correlations connecting points i and j are $I_{ij} - 1$, while solid correlations are I_{ij} . Further terms can be read immediately from the diagrams.

An example of this algorithm is shown in Fig. (4).

We furthermore enumerate some properties of Dyck paths, which therefore unveils the general properties of \mathcal{K}_N :

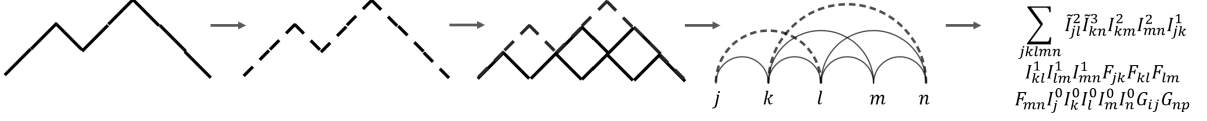


FIG. 4. Visual schematic of the algorithm to convert Dyck diagrams into terms in \mathcal{K} .

1. The set of all Dyck paths of order n has Narayana's number, $Nr(n, k)$, the number of paths with k peaks. The number of peaks is the multiplicity of \tilde{I} in the term. $Nr(n, k)$ is given by

$$Nr(n, k) = \frac{1}{n} \binom{n}{k} \binom{n}{k-1} \quad (\text{A39})$$

It is not difficult to show that $\sum_k Nr(n, k) = C_n$.

2. The number of Dyck paths in the set of all Dyck paths of order n having k number of segments is given by Catalan's triangle $C(n, k)$:

$$C(n, k) = \frac{n-k+1}{n+1} \binom{n+k}{k}. \quad (\text{A40})$$

In particular, if $n = k$, $C(n, n)$ is the n th Catalan's number C_n .

3. The number of Dyck paths in the set of all Dyck paths of order n having no hills (a segment of height 1), that is those with no \tilde{I}_1 term, is given by the Fine numbers F_n with generating function $F(x)$ ⁶⁸:

$$F(x) = \sum_{n \geq 0} F_n x^n = \frac{1 - \sqrt{1-4x}}{x(3 - \sqrt{1-4x})}. \quad (\text{A41})$$

This distribution also describes (1) Dyck paths where the leftmost peak is of even height,⁶⁸ and (2) the number of even returns to the horizontal axis (valley of height 0)⁶⁸.

4. The number of Dyck paths in the set of all Dyck paths of order $2n + 2m$ with m returns to the horizontal axis is given by the Ballot numbers $B(n, m)$

$$B(n, m) = \frac{m-n}{m+n} \binom{m+n}{n}, \quad (m, n) \neq (0, 0) \quad (\text{A42})$$

5. The number of Dyck paths in the set of all Dyck paths of order n with k occurrences of different $\nearrow \searrow \nearrow$ is given by $T(n, k)$, where $T(n, k)$ is related to Motzkin's number $M(k)$ via⁶⁹

$$T(n+1, k) = \binom{n}{k} M(n-k). \quad (\text{A43})$$

Particularly, the generator of Motzkin's number $M(k)$, $m(x) = \sum_0^\infty M(n)x^n$, satisfies

$$x^2 m(x)^2 + (x-1)m(x) + 1 = 0. \quad (\text{A44})$$

6. The number of Dyck paths in the set of all Dyck paths of order n whose peaks' height total to k can be read off from Triangle A094449.⁷⁰

Further properties of the Dyck paths have been enumerated in great detail in the On-Line Encyclopedia of Integer Sequences⁷⁰. To construct the memory kernels via this approach, we can represent Dyck paths as Dyck Words. \nearrow becomes 1 and \searrow becomes 0. Hence, the Dyck path in Fig. (4) is 11011000. By representing each path by a bit string, we can write an efficient code that enumerates all possible Dyck paths of order N . The conversion code is available upon request.

Appendix C. DETAILS ON COMPUTING $J(\omega)$ FROM $\rho(t)$

We provide more details on the inverse extraction procedure that goes from reduced system dynamics, $\rho(t)$, to the bath spectral density, $J(\omega)$. We show that such a map is nearly bijective in that any aspects of $J(\omega)$ that affect the reduced system dynamics can be obtained by analyzing $\rho(t)$. This construction has a direct connection with Hamiltonian learning literature, as pointed out in our main text.

To proceed, we recall

$$\rho \leftrightarrow \mathbf{U} \leftrightarrow \mathcal{K} \leftrightarrow \mathbf{I} \leftrightarrow \eta \leftrightarrow J(\omega). \quad (\text{A45})$$

We will explain step-by-step how to go from left to right. First, to obtain \mathbf{U}_N from ρ_N note that $\rho_N = \mathbf{U}_N \rho_0$, where ρ_N is a vector in Liouville space with a dimension of N_L . \mathbf{U}_N is then a $N_L \times N_L$ matrix. With N_L linearly-independent trajectories (obtained experimentally or computationally), we can uniquely determine \mathbf{U}_N . We then stack them to make the matrix

$$\mathbf{P}_N = [\rho_N^{(1)} | \rho_N^{(2)} | \dots | \rho_N^{(N_L)}]. \quad (\text{A46})$$

With this definition, we arrive at a simple linear equation to solve,

$$\mathbf{P}_N = \mathbf{U}_N \mathbf{P}_0 \quad (\text{A47})$$

By inverting \mathbf{P}_0 , we obtain

$$\mathbf{U}_N = \mathbf{P}_N \mathbf{P}_0^{-1}. \quad (\text{A48})$$

\mathbf{P}_0 is invertible because each trajectory is generated from a linearly independent initial condition. While we only considered noise-free data inputs, if the data is noisy, one can use more trajectories than N_L (i.e., \mathbf{P}_N and \mathbf{P}_0 become a fat matrix) and perform the Moore-Penrose pseudoinverse, which could help mitigate noise.

To obtain \mathcal{K} from \mathbf{U} we decompose the latter iteratively, in the manner presented in the main text Eq. (6) and e.g., Ref. 41.

Next, we move to obtain \mathbf{I} from \mathcal{K} . First, we define $\tilde{\mathcal{K}}_N$ which is defined through $\mathbf{G} \tilde{\mathcal{K}}_N \mathbf{G} = \mathcal{K}_N$. From $\tilde{\mathcal{K}}_0$, we have

$$\Delta t^2 (\tilde{\mathcal{K}}_0 + \mathbf{G}^{-1} \mathbf{L} \mathbf{G}^{-1})_{ii} = I_{0,i} \quad (\text{A49})$$

Similarly, we have

$$\tilde{\mathcal{K}}_{1,jk} = \frac{1}{\Delta t^2} I_{0,j} F_{jk} \tilde{I}_{1,jk} I_{0,k} \Rightarrow \tilde{I}_{1,jk} = \Delta t^2 \frac{\tilde{\mathcal{K}}_{1,jk}}{F_{jk} \tilde{U}_{0,jj} \tilde{U}_{0,kk}}. \quad (\text{A50})$$

For $N = 2$, we have

$$\tilde{\mathcal{K}}_{2,jn} = \tilde{I}_{2,jn} \frac{1}{\Delta t^2} \sum_k F_{jk} F_{kn} I_{1,jk} I_{1,kn} I_{0,j} I_{0,k} I_{0,n} + \frac{1}{\Delta t^2} \sum_k F_{jk} F_{kn} \tilde{I}_{1,jk} \tilde{I}_{1,kn} I_{0,j} I_{0,k} I_{0,n}, \quad (\text{A51})$$

which leads to

$$\tilde{I}_{2,jn} = \frac{\Delta t^2 \tilde{\mathcal{K}}_{2,jn} - \sum_k F_{jk} F_{kn} \tilde{I}_{1,jk} \tilde{I}_{1,kn} I_{0,j} I_{0,k} I_{0,n}}{\sum_k F_{jk} F_{kn} I_{1,jk} I_{1,kn} I_{0,j} I_{0,k} I_{0,n}}. \quad (\text{A52})$$

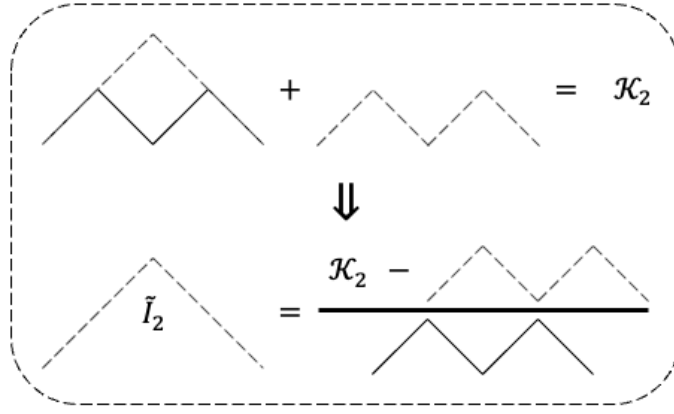
This procedure is, in fact, diagrammatically generalizable—its diagrammatic equation is shown in Fig. (5). One can generate all Dyck diagrams (which can be translated into a particular term in \mathcal{K}_N) of order N . From the sum of all diagrams, one moves all diagrams except the crest term to the side of \mathcal{K}_N . The crest term corresponds to the diagram that contains $\tilde{\mathbf{I}}_N$. Then, one divides both sides of the equation with the rest of the terms, which then yields $\tilde{\mathbf{I}}_N$.

Now to obtain η from \mathbf{I} , we start by taking the logarithm of Eq. (A8),

$$\ln I_{k'-k, x_k^\pm x_{k'}^\pm} = -(x_k^+ - x_k^-) (\eta_{kk'} x_{k'}^+ - \eta_{kk'}^* x_{k'}^-). \quad (\text{A53})$$

Here, we consider the spin-boson model with σ_z coupling, so $x^\pm \in \text{pair}\{+1, -1\}$. In this example, we have

$$\ln I_{(k'-k)[1,-1][1,-1]} = 4 \text{Re } \eta_{kk'} \quad (\text{A54})$$

FIG. 5. Visual schematic of the inversion diagram for \tilde{I}_2

$$\ln I_{(k'-k)[1,-1][1,1]} = 4i \operatorname{Im} \eta_{kk'}. \quad (\text{A55})$$

We can also readily obtain η_{kk} from I_0 through a similar manner.

Lastly, to obtain the spectral density, $J(\omega)$, we recall that (for clarity $k - k' \rightarrow \Delta k$)

$$\eta_{\Delta k} = \int_{-\infty}^{\infty} d\omega \mathcal{F}(\omega) e^{-i\omega \Delta t \Delta k}. \quad (\text{A56})$$

where

$$\mathcal{F}(\omega) = \frac{2}{\pi} \frac{J(\omega)}{\omega^2} \frac{\exp\{\beta \hbar \omega / 2\}}{\sinh \beta \hbar \omega / 2} \sin^2(\omega \Delta t / 2) \quad (\text{A57})$$

Note, in practice, we construct $\eta_{\Delta k}$ from $I_{kk'}$ for $\Delta k > 0$ and take the hermitian conjugate of $\eta_{\Delta k}$ for $\Delta k < 0$. We use I_{kk} for η_0 . To extract $\mathcal{F}(\omega)$ with the knowledge of $\eta_{\Delta k}$ we perform a Fourier Transform

$$\mathcal{F}(\omega) = \frac{1}{2\pi} \int_{-\infty}^{\infty} dt \eta_{\Delta k} e^{i\omega \Delta t \Delta k}, \quad (\text{A58})$$

which, in practice, is performed via a discrete Fourier transform

$$\mathcal{F}(\omega) = \frac{\Delta t}{2\pi} \sum_{\Delta k = -\Delta k_{\max}}^{\Delta k_{\max}} \eta_{\Delta k} e^{i\omega \Delta t \Delta k}. \quad (\text{A59})$$

This immediately gives the spectral density through

$$J(\omega) = \mathcal{F}(\omega) \frac{\pi \omega^2 \sinh \beta \hbar \omega / 2}{2 \sin^2(\omega \Delta t / 2) \exp\{\beta \hbar \omega / 2\}}. \quad (\text{A60})$$

One must pay special attention to frequencies with $\omega \Delta t / 2 = n\pi$ for integer n as the denominator in Eq. (A60) is zero. This is not a problem because the spectral density at such ω values does not alter the reduced system dynamics as they do not contribute to $\mathcal{F}(\omega)$ as shown in Eq. (A59). Another case to consider is the pure dephasing limit where \hat{H}_S is diagonal and commutes with \hat{H}_I . In this case, only the real part of η is available,

$$\begin{aligned} \operatorname{Re} \eta(\Delta k) &= \operatorname{Re} \int_{-\infty}^{\infty} d\omega \mathcal{F}(\omega) e^{-i\omega \Delta t \Delta k} \\ &= \int_{-\infty}^{\infty} d\omega \mathcal{F}(\omega) \cos \omega \Delta t \Delta k. \end{aligned} \quad (\text{A61})$$

We can then perform the inverse cosine transform to obtain $\mathcal{F}(\omega)$,

$$\mathcal{F}(\omega) = \frac{1}{\pi} \int_{-\infty}^{\infty} d\omega \operatorname{Re} \eta(\Delta k) \cos \omega \Delta t \Delta k. \quad (\text{A62})$$

Appendix D. THE DRIVEN OPEN QUANTUM SYSTEM

Here, we consider the explicit time dependence in the system Hamiltonian. We start by inspecting the INFPI formalism without assuming any time-translational invariance of any tensors:

$$\begin{aligned} U_{k,0,x_{2k}^\pm x_0^\pm} &= \sum_{x_{2k-1}^\pm} G_{2k-1,x_{2k}^\pm x_{2k-1}^\pm} \sum_{x_1^\pm} \tilde{U}_{k-1,0,x_{2k-1}^\pm x_1^\pm} G_{0,x_1^\pm x_0^\pm}, \\ F_{2k-1,x_{2k+1}^\pm x_{2k-1}^\pm} &= \sum_{x_{2k}^\pm} G_{2k,x_{2k+1}^\pm x_{2k}^\pm} G_{2k-1,x_{2k}^\pm x_{2k-1}^\pm}, \end{aligned} \quad (\text{A63})$$

with $G_{m,x_{m+1}^\pm x_m^\pm} = \langle x_{m+1}^+ | e^{-\frac{i\hat{H}_s(t_m/2)\Delta t}{2}} | x_m^+ \rangle \langle x_m^- | e^{\frac{i\hat{H}_s(t_m/2)\Delta t}{2}} | x_{m+1}^- \rangle$. There, $\hat{H}_s(t_m)$ is the system Hamiltonian at time $t_m = m\Delta t$. Hence,

$$\tilde{U}_{0,0,x_1^\pm x_1^\pm} = I_{0,x_1^\pm} \quad (\text{A64})$$

$$\begin{aligned} \tilde{U}_{1,0,x_3^\pm x_1^\pm} &= F_{1,x_3^\pm x_1^\pm} I_{1,x_3^\pm x_1^\pm} I_{0,x_3^\pm} I_{0,x_1^\pm} \\ \tilde{U}_{2,0,x_5^\pm x_1^\pm} &= \sum_{x_3^\pm} F_{3,x_5^\pm x_3^\pm} F_{1,x_3^\pm x_1^\pm} I_{2,x_5^\pm x_1^\pm} I_{1,x_5^\pm x_3^\pm} I_{1,x_3^\pm x_1^\pm} I_{0,x_5^\pm} I_{0,x_3^\pm} I_{0,x_1^\pm}. \end{aligned} \quad (\text{A65})$$

Similarly, the memory kernels are no longer time-translationally invariant. Consider

$$\mathcal{K}_{0,0} = \mathbf{U}_{1,0} - \mathbf{L}_0 \quad (\text{A66})$$

$$\mathcal{K}_{1,0} = \mathbf{U}_{2,0} - \mathbf{L}_1 \mathbf{U}_{1,0} - \mathcal{K}_{1,1} \mathbf{U}_{1,0} \quad (\text{A67})$$

where $\mathbf{L}_n \equiv (\mathbf{1} - \frac{i}{\hbar} \mathcal{L}_{S,n} \Delta t)$ with $\mathcal{L}_{S,n} \bullet \equiv [\hat{H}_S(n\Delta t), \bullet]$. We also have

$$\mathcal{K}_{1,1} = \mathbf{U}_{2,1} - \mathbf{L}_1 \quad (\text{A68})$$

Hence,

$$\mathcal{K}_{1,0} = \mathbf{U}_{2,0} - \mathbf{U}_{2,1} \mathbf{U}_{1,0}. \quad (\text{A69})$$

This allows us to write $\mathcal{K}_{1,0}$ in terms of \mathbf{I} :

$$\begin{aligned} (\mathcal{K}_{1,0})_{im} &= \frac{1}{\Delta t^2} \left[\sum_j G_{3,ij} \sum_k F_{1,jk} I_{1,jk} I_{0,j} I_{0,k} G_{0,km} - \sum_j G_{3,ij} I_{0,j} \sum_k G_{1,jk} \sum_l G_{1,kl} I_{0,l} G_{0,lm} \right] \\ &= \frac{1}{\Delta t^2} \left[\sum_j G_{3,ij} \sum_k F_{1,jk} I_{1,jk} I_{0,j} I_{0,k} G_{0,km} - \sum_j G_{3,ij} I_{0,j} \sum_k F_{1,jk} I_{0,k} G_{0,km} \right] \\ &= \frac{1}{\Delta t^2} \left[\sum_{jk} G_{3,ij} F_{1,jk} (I_{1,jk} - 1) I_{0,j} I_{0,k} G_{0,km} \right]. \end{aligned} \quad (\text{A70})$$

Inspecting equations for later time \mathcal{K} , we observed that the structure of the \mathcal{K} remains largely unchanged except for including time indices for the bare system propagators. In particular, we collect all the terms except the time-dependent ones (only the bare system propagators) as a tensor, which is time-translational. That is,

$$\mathcal{K}_{1+s,s;im} = \frac{1}{\Delta t^2} \left[\sum_{jk} \underbrace{G_{s+3,ij} F_{s+1,jk} G_{s,km}}_{P_{ijkm}^{s+2,s}} T_{1,jk} \right], \quad (\text{A71})$$

$$\mathcal{K}_{2+s,s;ip} = \frac{1}{\Delta t^2} \sum_{jkn} \underbrace{G_{s+5,ij} F_{s+3,jk} F_{s+1,kn} G_{s,np}}_{P_{ijknp}^{s+3,s}} T_{2,jkn}, \quad (\text{A72})$$

where $T_{1,jk} = (I_{1,jk} - 1) I_{0,j} I_{0,k}$, $T_{2,jkn} = (\tilde{I}_{2,jn} I_{1,jk} I_{1,kn} + \tilde{I}_{1,jk} \tilde{I}_{1,kn}) I_{0,j} I_{0,k} I_{0,n}$.

For problems with driven Hamiltonians, methods relying on time-translational invariance of memory kernels such as TTM become inapplicable to apply since the transfer tensor depends explicitly on time. Other schemes that

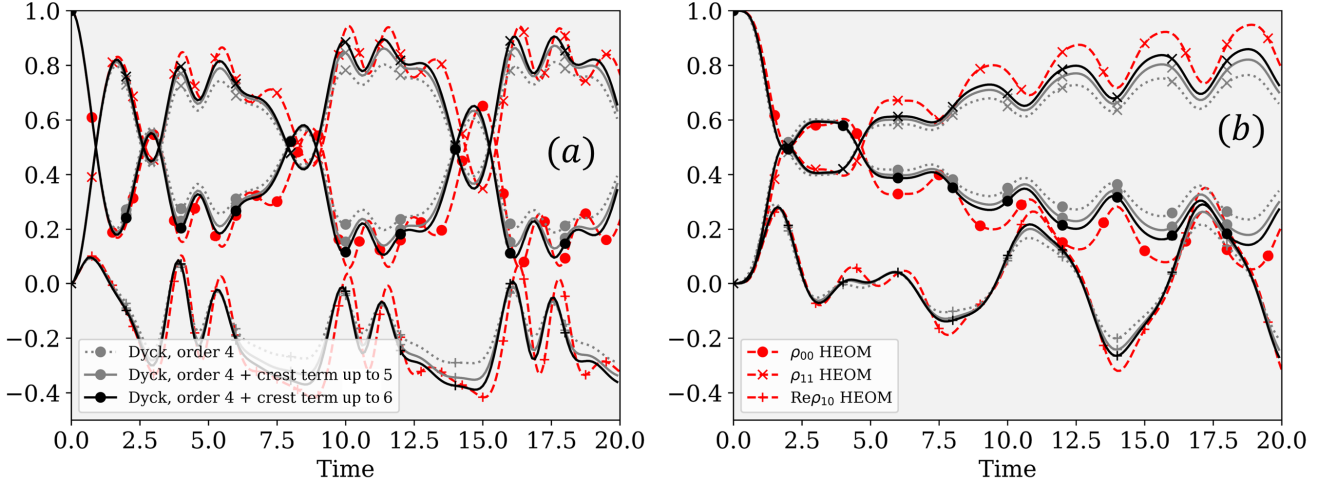


FIG. 6. Dynamics of various driven systems open to a thermal bosonic environment. Parameters used are: $\Delta = \epsilon = 1$ (other parameters are expressed relative to $\Delta = \epsilon$), $\beta = 5$, $\Delta t = 0.1$, $\omega_c = 7.5$, and $\xi = 0.1$. The memory kernel is truncated at the 4th timestep for the Dyck diagrammatic method (dashed) with an additional leading term correction, the diagrams with the highest heights (smallest multiplicity), upto the sixth timestep (solid). These trajectories are compared to the exact HEOM results.

treat this problem^{24,71} seem limited to invoking periodicity and temporal symmetries at least in terms of numerical efficiency. Here, we devise an efficient procedure to perform reduced system dynamics, exploiting the time-translational symmetry of the T s. The plan goes as follows: One computes all the T^i up until a predefined truncation parameter $i = r_{\max}$. Then, to obtain the kernel at time j one performs a tensor contraction with the time-dependent bare system propagator tensor, which is trivial to obtain.

As a proof of concept, we consider various driven systems in Fig. (6), where in panel (a): $\hat{H}_s = (\epsilon - \sin(t))\sigma_z + \sigma_x$, and in panel (b): $\hat{H}_s = \epsilon\sigma_z + \sin(t)\sigma_x$. In these results, we include all Dyck diagrams up to the fourth order to compute \mathcal{K}_0 to \mathcal{K}_4 . We then approximate \mathcal{K}_5 and \mathcal{K}_6 by including only the diagram with the smallest multiplicity (i.e., the crest term), which is justified since the coupling here is weak and so $\tilde{I} \ll 1$. We observe that while the order 4 Dyck diagrammatic method captures the main features of the exactly computed driven dynamics (with HEOM), it is still not converged. After we include leading order correction terms up to 6 (including only the diagram with the highest height), we observe that the Dyck diagrammatic method converges to the exact values.

In panel (a), the diagonal elements of the Hamiltonian are driven. As expected, we see a lot of interlevel population crossing here. This is to be contrasted with panel (b), where the population of ρ_{11} is mostly larger than ρ_{00} except for some initial time. We also observe that for the latter, the oscillations of the populations are more regular.

Appendix E. HEOM CALCULATIONS

All hierarchical equations of motion (HEOM)^{63,64} calculations presented in this work made use of the free pole HEOM variant,³¹ which makes use of the adaptive Antoulas–Anderson (AAA) algorithm⁷² for constructing a simple rational function approximation to the bath noise spectrum,

$$S(\omega) = \frac{1}{2}J(\omega) \left[\coth\left(\frac{\beta\omega}{2}\right) + 1 \right] \quad (\text{A73})$$

which, in turn, gives rise to a sum of exponential functions representation of the bath correlation function

$$C(t) \approx \sum_{j=1}^K \alpha_k e^{-\nu_k t}, \quad (\text{A74})$$

with $\text{Re}(\nu_k) \geq 0$. The HEOM approach makes use of the Feynman–Vernon influence functional discussed in [Appendix A](#), to obtain a description of the exact dynamics of an open quantum system in terms of an infinite hierarchy of auxiliary density operators (ADOs), $\hat{\rho}_{\mathbf{m},\mathbf{n}}(t)$, that encode the system–bath correlations. These ADOs are indexed by

two sets of integers $\mathbf{m} = (m_0, m_1, \dots, m_K)$ and $\mathbf{n} = (n_0, n_1, \dots, n_K)$, each of length K .³¹ For practical calculations, this hierarchy is truncated such that no element of \mathbf{m} or \mathbf{n} is greater than some integer L .

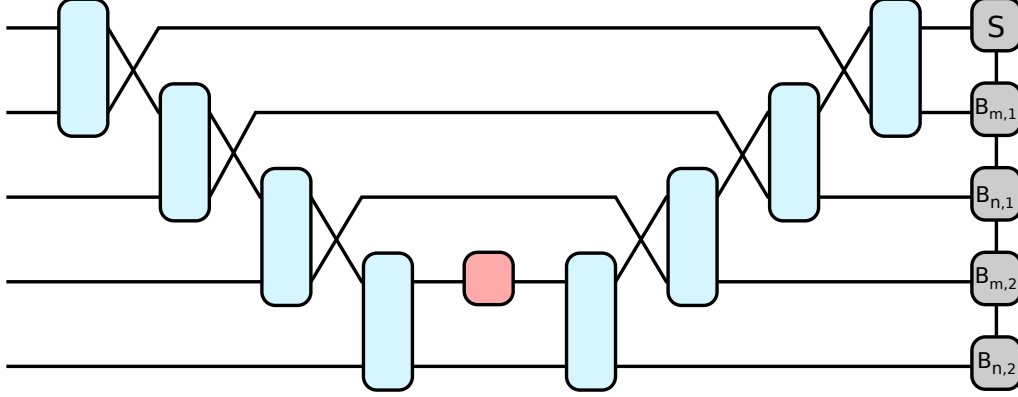


FIG. 7. An illustration of a single time step of the swap based two-site TEBD algorithm used to integrate the FP-HEOMs. Crossing of lines indicates a swap operation applied to the MPS state. The grey rectangles represent the MPS representation of the hierarchy of ADOs, $\hat{\rho}$. The light blue rectangles correspond to the short time bath propagators, $\mathcal{B}_{m,k}$, $\mathcal{B}_{n,k}$, and red rectangles correspond to the short time system propagator term, $\mathcal{U}_S(t)$.

Within the FP-HEOM method, this hierarchy of ADOs evolves according to the equations of motion³¹

$$\begin{aligned} \frac{\partial}{\partial t} \hat{\rho}_{\mathbf{m},\mathbf{n}}(t) = & - \left(i\mathcal{L}_s(t) + \sum_{k=1}^K (\nu_k m_k + \nu_k^* n_k) \right) \hat{\rho}_{\mathbf{m},\mathbf{n}}(t) - i \sum_{k=1}^N \left(\sqrt{\frac{m_k}{\|\alpha_k\|}} \alpha_k \hat{S} \hat{\rho}_{\mathbf{m}_k^-, \mathbf{n}}(t) - \sqrt{\frac{n_k}{\|\alpha_k\|}} \alpha_k^* \hat{\rho}_{\mathbf{m}, \mathbf{n}_k^-}(t) \hat{S} \right) \\ & - i \sum_{k=1}^N \left(\sqrt{(m_k+1)\|\alpha_k\|} \left[\hat{S}, \hat{\rho}_{\mathbf{m}_k^+, \mathbf{n}}(t) \right] + \sqrt{(n_k+1)\|\alpha_k\|} \left[\hat{S}, \hat{\rho}_{\mathbf{m}, \mathbf{n}_k^+}(t) \right] \right), \end{aligned} \quad (\text{A75})$$

where \mathbf{m}_k^\pm (\mathbf{n}_k^\pm) corresponds to the set of indices \mathbf{m} (\mathbf{n}) but with the k -th element incremented (+) or decremented (-) by one. These equations have the general form

$$\begin{aligned} \frac{\partial}{\partial t} \hat{\rho}(t) = & - i\mathcal{L}_s(t) \hat{\rho}(t) + \sum_{k=1}^N [\mathcal{L}_{m,k} + \mathcal{L}_{n,k}] \hat{\rho}(t) \\ = & \mathcal{M}(t) \hat{\rho}(t), \end{aligned} \quad (\text{A76})$$

where $\mathcal{L}_{m,k}$ is an operator that acts on system and the k -th mode of the hierarchy of ADOs.

For the ohmic and subohmic spectral densities with exponential cutoffs considered in this work, the total number of exponentials in the sum of exponential representation of the bath correlation function leads to a set of auxiliary density operators that are too large to represent exactly. Following references 31, 73, and 74 we use a matrix product state (MPS) representation of the ADOs. Evolution of the HEOMs is performed through the use of a two-site time-evolving block decimation (TEBD) algorithm that makes use of a symmetric Trotter splitting of the short-time HEOM propagator,

$$\begin{aligned} \mathcal{U}_{\text{heom}}(t, t + \Delta t) = & \mathcal{T} \exp \left(\int_t^{t+\Delta t} \mathcal{M}(\tau) d\tau \right) \\ \approx & \left(\prod_{k=1}^K \exp \left[\mathcal{L}_{m,k} \frac{\Delta t}{2} \right] \exp \left[\mathcal{L}_{n,k} \frac{\Delta t}{2} \right] \right) \exp \left[-i\mathcal{L}_S \left(t + \frac{\Delta t}{2} \right) \frac{\Delta t}{2} \right] \left(\prod_{k=K}^1 \exp \left[\mathcal{L}_{n,k} \frac{\Delta t}{2} \right] \exp \left[\mathcal{L}_{m,k} \frac{\Delta t}{2} \right] \right) \\ = & \left(\prod_{k=1}^K \mathcal{B}_{m,k} \mathcal{B}_{n,k} \right) \mathcal{U}_s(t) \left(\prod_{k=K}^1 \mathcal{B}_{n,k} \mathcal{B}_{m,k} \right) \end{aligned} \quad (\text{A77})$$

In contrast to the single-site time-dependent variational principle-based schemes that have previously been used for the time evolution of tensor network-based approximations to the HEOMs,^{31,73-76} the use of a two-site TEBD scheme naturally allows for adaptive control of the MPS bond dimension throughout a simulation.

The interactions present in the HEOMs given in Eq. A75 have a star topology; terms acting on two modes of the system all act on the system degree of freedom as well as one of the modes of the hierarchy. The application of the propagator in Eq. A77 would require the application of two-body operators acting on modes that are not nearest-neighbor in the MPS, giving rise to an algorithm that requires $O(K^2)$ two-site updates at each time step. To avoid this overhead, we employ a strategy where at the application of each two-body term, we swap the position of the system and bath site being acted upon, ensuring that at each stage the next two-body operator to apply is a local operation on the MPS.^{77,78} This update scheme is illustrated schematically in Fig. 7, and requires $O(K)$ two-site updates at each time step. This scheme has the advantage that at each stage, we perform a TEBD update between the system site and a single bath site. Consequentially, when the system Liouville space dimension is much smaller than the hierarchy depth, the cost of two-site updates will be dramatically reduced compared to the naive approach.

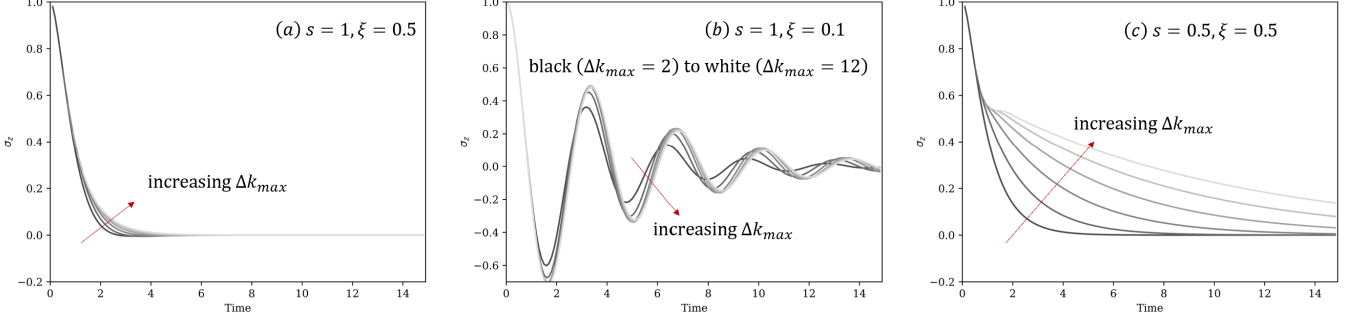


FIG. 8. Magnetization ($\langle\sigma_z(t)\rangle$) dynamics predicted using i-QuAPI method with increasing Δk_{\max} (from black to white colors, $\Delta k_{\max} = 2$ to $\Delta k_{\max} = 12$). Parameters used are: $\Delta = 1$, $\epsilon = 0$, $\beta = 5$, $\Delta t = 0.1$, $\omega_c = 7.5$, and $\xi = 0.1$ and $s = 1$ (panel (a)), $\xi = 0.5$ and $s = 1$ (panel (b)), or $\xi = 0.5$ and $s = 0.5$ (panel (c))

Appendix F. ADDITIONAL SIMULATIONS

For Figures (2) and (3) panels (a) and (b), the exact results from which our calculations compare come from converged HEOM results. We cross-validate these results using the i-QuAPI method, which agrees with HEOM, see Fig. (8).

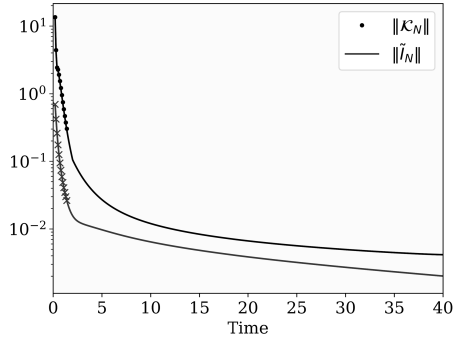


FIG. 9. Same as Fig. 2 with a longer time.

Fig. (2) panel (c) suggests that the decay of $\|\tilde{\mathbf{I}}_N\|$ (and hence $\|\mathcal{K}_N\|$) is extremely slow. One question is if they eventually decay to zero at all. In Fig. (9) we present $\|\tilde{\mathbf{I}}_N\|$ and $\|\mathcal{K}_N\|$ for longer times than in the main text. We observe that neither has vanished and both are still decaying even until $t = 40$.

In Fig. (10), we demonstrate the perfect agreement between inversely obtained η to the analytical η . This is the intermediate step to extract the spectral density of the environment, see Appendix C.

Furthermore, we show how we can inversely obtain $J(\omega)$ for highly structured environments in Fig. 11: in panel (a) $J_a(\omega) = \frac{\gamma\omega\omega_0^2}{(\omega^2 - \omega_0^2)^2 + \gamma^2\omega^2} + \frac{\gamma\omega\omega_0^2}{(\omega^2 - 4\omega_0^2)^2 + \gamma^2\omega^2}$, for panel (b) $J_b(\omega) = \frac{\gamma}{(\omega - \omega_0)^2 + \gamma^2} + \frac{\gamma}{(\omega - 3\omega_0)^2 + \gamma^2}$, and for panel (c)

$J_c(\omega) = \frac{\gamma\omega\omega_0^2}{(\omega^2-\omega_0^2)^2+\gamma^2\omega^2} + \frac{\gamma}{(\omega-3\omega_0)^2+\gamma^2}$. Specifically these are spectral densities that are the additions of brownian-brownian, lorentz-lorentz, and brownian-lorentz spectral densities with different peak frequencies, respectively. It is significant that even for highly structured spectral densities such as these the extraction procedure succeeds, although one would need to go to high orders in the Dyck diagrams.

Lastly, we look at how the truncation in \mathcal{K} affects \mathbf{I} and vice versa. We construct approximate \mathcal{K} with truncated $\tilde{\mathbf{I}}$ (i.e., akin to i-QUAPI). Similarly, we extract effective \mathbf{I} with truncated \mathcal{K} (i.e., akin to GQME). We present these results in Fig. (12). Here, we study the three different regimes considered in the main text. In panels (a1), (b1), and (c1), we show the decay of $\|\mathcal{K}_N\|$ of Dyck order 13, if we truncate (set $\tilde{\mathbf{I}}_{k,ij} = 0$ for $k > k_{\max}$) at $k_{\max} = 5$, $k_{\max} = 9$, and $k_{\max} = 13$ respectively. Here, one observes the error of premature truncation compounds, at e.g., $t = 1.2$ the error of $\|\mathcal{K}_N\|$ when truncating at $k_{\max} = 5$ is significantly larger than when truncating at $k_{\max} = 9$. On the other hand, it appears that the effective $\tilde{\mathbf{I}}$ extracted from this truncated \mathcal{K} is a poor approximate of the actual $\tilde{\mathbf{I}}$ (although this makes sense since we impose a hard truncation, $\tilde{\mathbf{I}}_{k,ij} = 0$ for $k > k_{\max}$). This is shown in panels (a2), (b2), and (c2); of Dyck order 13, at $k_{\max} = 5$, $k_{\max} = 9$, and $k_{\max} = 13$, respectively.

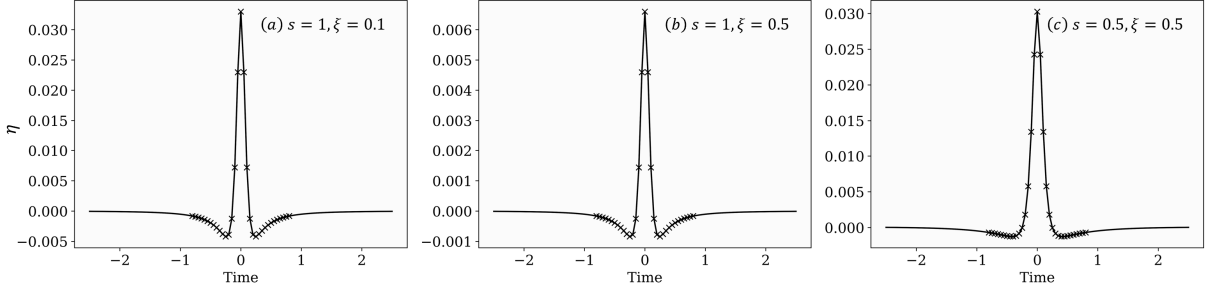


FIG. 10. The coefficients $\eta_{\Delta k}$ inversely calculated (solid line), which perfectly matches the a priori results (crosses). Parameters are identical to Fig. 3 in the main text.

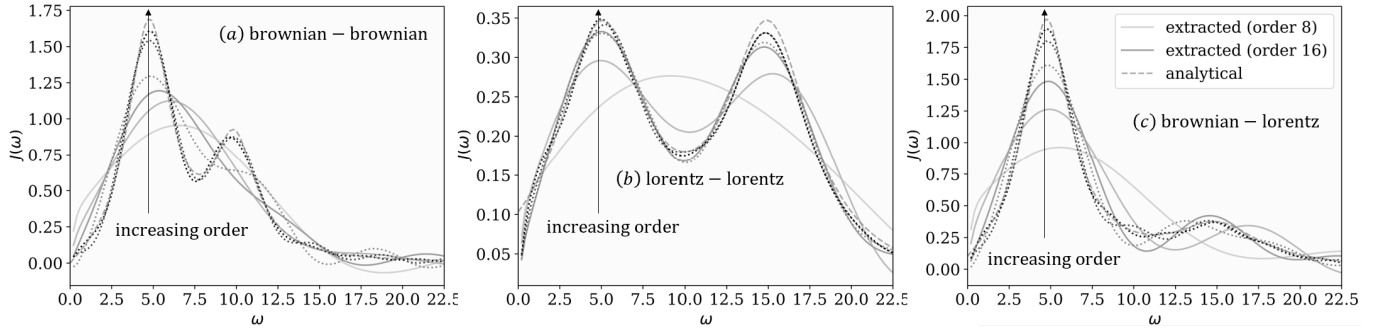


FIG. 11. Panels (a), (b), and (c): Bath spectral densities extracted through the Dyck diagrammatic method with increasing truncation orders (from white to black colors, 8, 12, 16, 20, 30, and 40 in sequence) compared to exact spectral densities (dashed), see Appendix C. Note that for orders 20, 30, and 40 (dotted), we directly proceed from $\mathbf{I} \rightarrow \eta \rightarrow J(\omega)$ since the procedure $\mathcal{K} \rightarrow \mathbf{I}$ for these high orders are currently infeasible. In all cases, our approach obtains the structured spectral density. For panel (a) the exact spectral density $J_a(\omega) = \frac{\gamma\omega\omega_0^2}{(\omega^2-\omega_0^2)^2+\gamma^2\omega^2} + \frac{\gamma\omega\omega_0^2}{(\omega^2-4\omega_0^2)^2+\gamma^2\omega^2}$, for panel (b) $J_b(\omega) = \frac{\gamma}{(\omega-\omega_0)^2+\gamma^2} + \frac{\gamma}{(\omega-3\omega_0)^2+\gamma^2}$, and for panel (c) $J_c(\omega) = \frac{\gamma\omega\omega_0^2}{(\omega^2-\omega_0^2)^2+\gamma^2\omega^2} + \frac{\gamma}{(\omega-3\omega_0)^2+\gamma^2}$. Parameters used are: $\Delta = 1$ (other parameters are expressed relative to Δ), $\epsilon = 0$, $\beta = 5$, $\Delta t = 0.05$, $\omega_c = 7.5$, $\xi = 2$, $\gamma = \frac{\xi\pi}{2}$, and $\omega_0 = 5$.

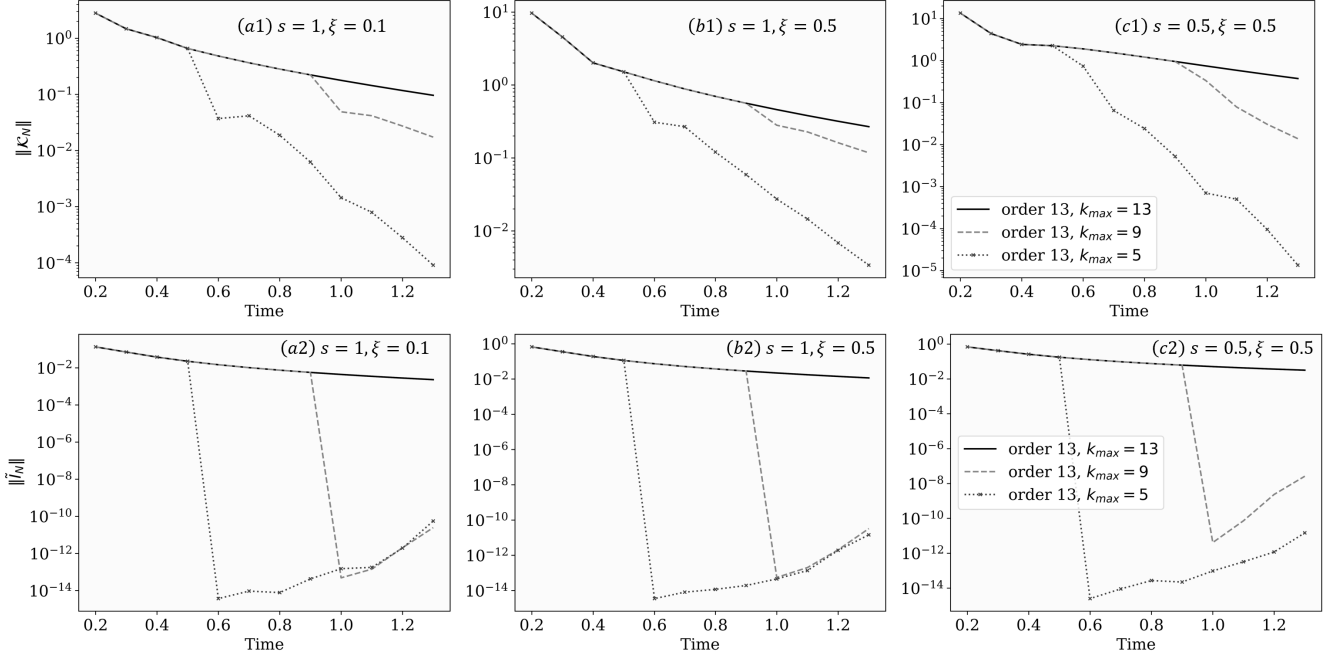


FIG. 12. Panels (a1), (b1), and (c1): The operator norm of the approximate \mathcal{K}_N when we truncate (set $\tilde{I}_{k,ij} = 0$ for $k > k_{\max}$) at $k_{\max} = 5$, $k_{\max} = 9$, and $k_{\max} = 13$, respectively. The solid line is the exact \mathcal{K}_N . Panels (a2), (b2), and (c2): The operator norm of $\tilde{\mathbf{I}}_N$ obtained from approximate \mathcal{K}_N shown in panels (a1), (b1), and (c1). The solid line indicates the exact $\tilde{\mathbf{I}}_N$. Parameters used are: $\Delta = 1$ (other parameters are expressed relative to Δ), $\epsilon = 0$, $\beta = 5$, $\Delta t = 0.1$, $\omega_c = 7.5$, and $\xi = 0.1$ and $s = 1$ (panel (a)), $\xi = 0.5$ and $s = 1$ (panel (b)), or $\xi = 0.5$ and $s = 0.5$ (panel (c))